BRNO UNIVERSITY OF TECHNOLOGY

VYSOKÉ UČENÍ TECHNICKÉ V BRNĚ

FACULTY OF MECHANICAL ENGINEERING

FAKULTA STROJNÍHO INŽENÝRSTVÍ

ENERGY INSTITUTE

ENERGETICKÝ ÚSTAV

NUMERICAL INVESTIGATION OF TRANSPORT AND DEPOSITION OF FIBROUS AEROSOL IN SIMPLIFIED MODEL OF RESPIRATORY SYSTEM

NUMERICKÉ SIMULACE TRANSPORTU A DEPOZICE VLÁKEN V ZJEDNODUŠENÉM MODELU DÝCHACÍCH CEST

MASTER'S THESIS

DIPLOMOVÁ PRÁCE

AUTHOR
AUTOR PRÁCE

Usman Masood

SUPERVISOR
VEDOUCÍ PRÁCE

Ing. Jakub Elcner, Ph.D.

BRNO 2023

Assignment Master's Thesis

Institut:	Energy Institute
Student:	**Usman Masood**
Degree programm:	Mechanical Engineering
Branch:	no specialisation
Supervisor:	**Ing. Jakub Elcner, Ph.D.**
Academic year:	2022/23

As provided for by the Act No. 111/98 Coll. on higher education institutions and the BUT Study and Examination Regulations, the director of the Institute hereby assigns the following topic of Master's Thesis:

Numerical investigation of transport and deposition of fibrous aerosol in simplified model of respiratory system

Brief Description:

Numerical research in the field of non–spherical particles bears challenges in the form of the need to solve more complex interactions between particles dispersed in inhaled air. The Lagrangian approach, implemented in a variety of commercial CFD (computational fluid dynamics) software, can trace spherical particles and compute their trajectories resulting from the action of external forces. Fibres, due to their specific shape, require a more complex solution. Their actual drag in the ambient air is influenced by their shape and actual rotation angle. Although we can control the drag coefficient by prescribing a suitable equation, we are not able to analyse the actual angle of rotation of the particle and, based on this information, establish a link between the rotation angle and the current equation of the drag coefficient. The Discrete Element Method (DEM), as an extension of the Lagrangian approach, has this capability. It models each particle in discrete order and therefore it is capable of better analysis of the motion of the particle. However, this method was originally designed to simulate flow of granular materials characterized by high particle densities, where the interparticle interactions are of importance. The problem of transport and deposition of fibres in the human respiratory system is different, because significant interactions between fibres dispersed in the inhaled air do not need to be assumed. The aim of this work is to test the possibilities of the CFD approach for the above case, considering the computational requirements of the simulations, and to select the most appropriate procedure to analyse it depending on the chosen particle shape or modification of its physical properties.

Master's Thesis goals:

Analyse the capabilities of the DEM method in the selected CFD solver
Select the optimal method for numerical investigation of fibre transport and deposition
Perform simulation of fibre deposition on a simplified airway geometry

Recommended bibliography:

Tu, Jiyuan | Computational fluid and particle dynamic | 2013 | 978-94-007-4487-5 | 4337941204

Zikanov, Oleg | Essential computational fluid dynamics | 2010 | 978-0-470-42329-5 | 4337934826

HIRSCH, Ch. Numerical computation of internal and external flows. Volume 1, Fundamentals of computational fluid dynamics. 2nd ed. Amsterdam:

Elsevier, 2007, xx, 656 s., [19] s. barev. obr. příl. : il. ISBN 978-0-7506-6594-0.

HIRSCH, Charles. Numerical computation of internal and external flows. Volume 2, Computational methods for inviscid and viscous flows. Chichester: John Wiley, 1990, 691 s. : il. ISBN 0-471-92452-0.

Hinds, William C. | Aerosol technology : properties, behavio | 1999 | 0-471-19410-7 | 4337920336

Deadline for submission Master's Thesis is given by the Schedule of the Academic year 2022/23

In Brno,

L. S.

doc. Ing. Jiří Pospíšil, Ph.D.
Director of the Institute

doc. Ing. Jiří Hlinka, Ph.D.
FME dean

Acknowledgements

I would like to express my sincere gratitude towards my supervisor Dr. Jakub Elcner at the Brno University of Technology, for his constant support and motivation, guiding me in the right direction during this thesis. His insightful recommendations in the project have proven to be extremely helpful to me.

I would also like to thank Assoc. Prof. Lizal Frantisek for giving me an opportunity to visit the lab at Energy Institute of the Brno University of Technology and provide me with the technical information and experimental aspects of this thesis.

My sincere thanks to the examiner, Assoc. Prof. Pavel Charvát, for his valuable advice and for all the help when needed.

Finally, a big thanks to my parents for their unconditional love and continuous support.

Usman Masood, Brno, May 2023

Declaration of Authenticity

I hereby declare that I wrote my master's thesis "Numerical Investigation of Transport and Deposition of Fibrous Aerosols in Simplified Model of Respiratory System." independently and without outside assistance. I did not use any other sources apart from the ones stated in the bibliography and I have clearly cited all passages (including graphics, tables, etc.) in the thesis that were taken from other sources. This thesis has never been submitted in its current or similar form in any other degree program.

26 – 05 – 2023

Date

Usman Masood

Author 's Name and Surname

Table of Contents

Abstract

Rigid particles such as fiber particles, asbestos or MMMFs (man-made mineral fibers) are harmful to human health when inhaled because of their abundance in the atmosphere, composition, and ability to penetrate deep into human lungs. It can cause lung cancer and numerous other diseases according to the severity of the exposure. To address this inhalation phenomenon and complex maneuvers of these hazardous particles, it is vital to monitor their behaviour such as the nature of their transport, deposition, and trajectory which they attain during the inhalation conditions.

Many previous studies regarding particle transport and deposition in human respiratory airways involved spherical particles, however, this research includes non-spherical thin and elongated particles in computational domain. Therefore, STAR CCM+ software is used to conduct this research and initial boundary conditions are taken from the preliminary experiments done by Lizal Frantisek and other researchers at Brno University of Technology, they assembled a test rig to visualize the motion of glass fibers through a replica of human airways.

Fibers exhibit different aerodynamic behavior than spherical particles, causing different deposition patterns. To investigate this phenomenon, a computational fluid dynamics simulation setup is constructed in Simcenter STAR CCM+ using a model of the human airway. The discrete element method (DEM) is used because this is an extension of lagrangian approach (LA), which deals with discrete particle parcels and solves the equation of motion to determine the trajectory as they move through time and space as well as it deals with particle shape and collision behaviour. Based on the simulations, particle deposition in the respiratory tract model is studied and its results are analyzed.

Keywords

1. Introduction

Hazardous particles such as aerosols, asbestos and fiber particles can cause respiratory diseases and conditions such as pleural plaques, fibrosis, asbestosis, lung cancer, and mesothelioma (IARC, 1977; IARC, 2002; IARC,2012; NRC, 1984; Wagner et al., 1985; Suzuki and Kohyama, 1984). The toxicity of these hazardous particles depends on the chemical composition, deposition, and retention due to the shape in the respiratory tract. The chemical composition such as solubility and surface ions which interact with tissues can cause adverse health effects and deposition criteria include interception, inertial impaction, gravitational sedimentation, Brownian diffusion, electrostatic charge, and interception, they act collectively to cause a net deposition of particles throughout the respiratory tract according to the regional significance. Shape parameters such as length, width, radius, and diameter etc. determine the trajectory which they attain during their motion. [1,49,50,51,52,53]

The focus of this thesis is airborne fibrous particles, usually referred to as high aspect ratio particles which means their length vs. width ratio is at least 3:1. Other high aspect ratio particle shapes include particle clumps, cylindrical and flexible fibers etc. These particle size can be nanoscale (≤100 nm) or microscale (> 100 nm) in diameter. The aerodynamic behavior of these particles is controlled by their size, orientation, and density. Deposition, transportation, and trajectory tracking are all aspects of fiberous particle aerodynamic behavior. Evaluating this behavior can assist researchers in understanding how fiberous particles migrate through a certain phase, how they deposit onto surfaces, and how they interact with limits that can induce retention. To define the aerodynamic behavior of spherical particles, just one dimension (radius or diameter) is required. Whereas, on the other hand, cylindrical or clumps like shaped particles will have at least two dimensions which is length and diameter, or many dimensions if the shape is more complicated. [1]

To investigate fibrous particle transport and deposition characteristics in human airway, a two-phase flow numerical simulation is proposed in this research. The fluid phase is calculated by computational fluid dynamics (CFD) and the particle phase is calculated by lagrangian approach (LA). For elongated particle clumps, the most suitable approach is discrete element

method (DEM) as non-spherical particle tend to flip and their flipping behaviour could lead to the change in particle's drag force during the transport, which is one of important factor in this investigation. The discrete element method (DEM) was invented by Cundall and Strack [2] and it soon became authentically accurate and further developed into several other branches. But the main DEM approach follows Newton's second law to calculate the individual particle's motion. The DEM could consider friction, contact plasticity, gravity, cohesion, and other interactions, record the information of each individual particle during simulation such as position, velocity, forces exerted on, etc. Thus, it is preferred to use DEM approach coupled with CFD.[3]

To verify the approach chosen for this numerical investigation, parameters are taken from a preliminary experiment. Lizal (Lizal Frantisek, Matous Cabalka, Milan Maly, et al) performed an experiment in which he assembled a test rig for visualization and recording of flowing fiber particles in a replica of human trachea and the first bronchial bifurcation. To perform this test, commercially produced glass fibers were processed, dispersed, and introduced into the flow. He concluded that fiber particles can reach to the lower parts of the respiratory tract, even though their diameter can be very small, but their length can reach 30 or 50 μm. It is also stated that fiber particles alignment with the flow streamlines plays a crucial role in deposition, hence parallel orientation is preferential in laminar flow than that of fibers with perpendicular orientation, due to their dominant behaviour during gravitational settling. However, it is often treated as the combination of these two cases. [4]

The preliminary experiment of Lizal and calculations of Tian and Ahmadi (Tian and Ahmadi et al. 2013) showed that every bifurcation induced a flip in the fiber's orientation. The significant portion of fiber particles rotated and oriented perpendicular to the flow streamlines.[5] The proposed DEM approach evaluates the position, rotation and velocity of each fiber while considering the orientation and moment of inertia of each fiber. The complexity of this task originated when fibers particles interact with the fluid. In uniform flow, spherical particles only experience the drag force, whereas particles clumps or elongated particles experience transverse lift force, a pitching torque, and a counter-rotational torque. The intensity of these forces depends not only on Reynolds number but also on the angle of the axes of the fiber with the direction of the flow. [4]

3

For spherical particles, drag force is determined using the drag coefficient, however for fiber particles, a non-symmetric flow field produces a lift force on the fiber that is not aligned with the flow, and its magnitude is computed using the lift coefficient. When the center of pressure of the total aerodynamic force acting on the fiber does not correspond with the center of mass, pitching torque is formed, and this pitching torque is the cause of fiber rotation as well as collisions with walls and suspended particles. Coefficients can be used to determine counter rotational torque for rotations around the axis of symmetry and rotations around the axis perpendicular to the axis of symmetry. However, they were calculated for axisymmetric particles in a uniform flow. [6] [4]

The aim of this research is to perform the numerical simulation with the parameters of preliminary experiments done by Lizal on the Y model geometry and a realistic model of human respiratory tract. The challenging task is to determine the behaviour of fiber particles in turbulent flow which is computationally demanding. The results of this numerical simulation are then compared and analyzed.

2. Literature Review

2.1 Airborne Rigid Particles

Airborne rigid particles in the atmosphere are solid particles that do not easily deform and can float in the air for extended periods of time. These particles can vary in size, shape, and composition, and they can come from both natural and man-made sources.

2.1.1 Aerosols

Aerosols are one example of rigid particles; They are typically tiny particles. Aerosols can be natural or anthropogenic and have a significant impact on the environment. These aerosols can cause respiratory problems and other health issues. [7]
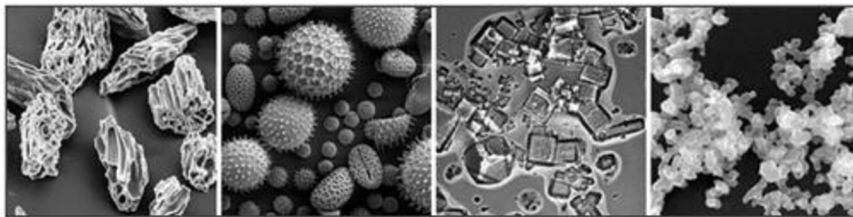
Figure 1: These are electron microscope images (not at the same scale) shows the wide variety of aerosols shapes. From Left to Right: Volcanic Ash, Pollen, Sea Salt, and Soot. [7]

2.1.2 Fiber Particles

Fiber particles are another type of rigid particles, they are usually elongated and thin particles with a diameter smaller than 3 μm, and a length larger than 5 μm, with the length-to-diameter ratio of 3:1 or more and is defined as respirable fibers in public healthcare by the World Health Organization (WHO, 2000). [8][48]

Fiber particles can also pose health concerns whether inhaled or swallowed. Numerous studies have revealed that the toxicity of fibers is not specific to the kind of mineral fiber, but rather to the length of the fibers, with fiber particles bigger than 5 μm being the most poisonous. The main sources of these fiber particles are industrial building materials, they are so small, they are only identified using a Scanning Electron Microscope with Energy Dispersive X-ray Spectroscopy (SEM-EDX). [8]

Fiber particles are classified into two types: organic fiber particles and inorganic fiber particles. The table below shows the detailed properties of these fiber particles. [8]

Table 1: Types and characteristics of fiber particles in air [8]

Fiber particle groups	Fiber particle types	Major elements	Morphologies
Organic	Microplastics	C, O (minor Ca, S, Mg, Al, Si)	Regular fibrous or spiral, smooth surface, mixed with other particles
	Natural organic	C, O (miner P)	Regular fibrous, surfaces non-uniform
Inorganic	Asbestos	Si, Mg, (minor, Al, Fe)	Regular fibrous or needlelike
	Calcium sulfate	S, Ca, and C	Regular fibrous
	MMMFs	Al, Si, Fe, Ca, Mg, S	Regular, irregular fibrous
	Metal	Fe, Ti, Mg, Na	Regular fibrous

All these particles are present in the atmosphere, they are respirable fibers and can be inhaled, their length size ranges from 5–600 μm, approximately 70% were in the range of 25–200 μm. [8]

The images of electron microscope of these fiber particles are shown in fig. 2. Natural organic fiber particle and its composition is shown in 2(g) and 2(j), elongated in shape and its surface is not uniform. Some natural organic fibers also had small particles attached. Carbon (C) and Oxygen (O) are their major elemental components, with minor component amount of P. Asbestos fiber particles in 2(b) and 2(e) have distinctive dimensions, it is needle-like morphology with smooth surface. MMMFs particles are regular fibrous bar shape in dimensions shown in 2(h). [8]

Microplastic and MMMFs fibers were most abundant in the atmosphere, accounting for 34.6% and 40.3% in total, respectively. Other particles are asbestos (7.8%), calcium sulfate (7.2%), metal fibers (5.6%) and natural organic fiber particles (4.5%). However, 80% of the airborne fiber particles between 5 μm and 20 μm were more easily suspended in the air and transported for a long distance. This size range of fibers is easily inhaled and can cause health risks, especially asbestos fibers, microplastic fibers and MMMFs [8].
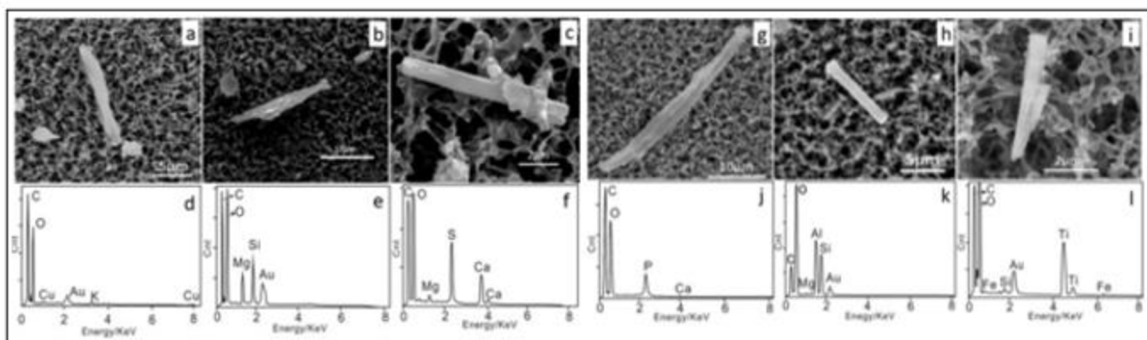
Figure 2: SEM images of airborne fiber particles and their composition, (a) Microplastic fiber, (b) asbestos, (c) CaSO4, (g) natural organic fiber, (h) MMMF, (i) Titanium metal fiber.[8]

2.2 Particle Deposition

The inhaled particles follow the complex route in the respiratory tract, they are posing to number of deposition mechanisms in their transport towards the deeper regions of the lungs. The main deposition mechanisms are inertial impaction, gravitational sedimentation, Brownian diffusion, turbulent flow regime, electrostatic precipitation, and interception as shown in fig.3. [9]

Figure 3: Deposition mechanism of inhaled particles in the lung, sites of deposition in the complex geometry of the respiratory tract. [9]

Inertial impaction is one of the primary methods of deposition, it happens when there is a sudden change in the direction of flow, causing the particles to deviate from the flow streamlines due to inertia, depending on the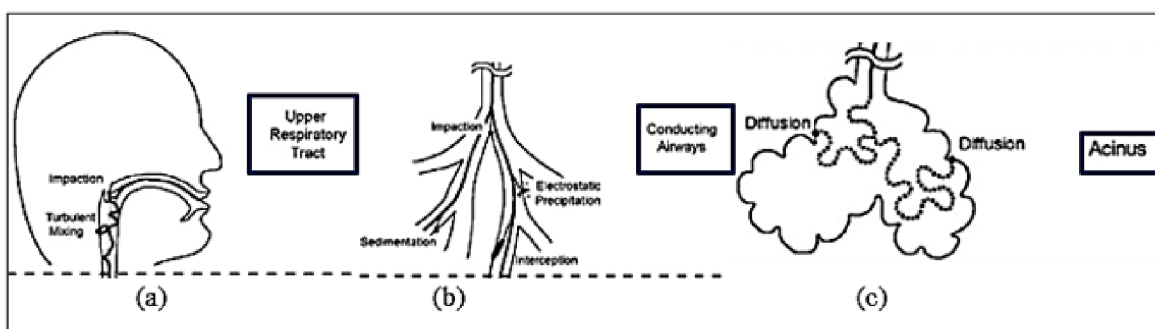 flow rate particles size influence the deposition, which cause them to collide with the walls of the tract and eventually they ejected from the flow and settle there. Secondly, gravitational sedimentation is a settlement of particles under gravitational force, when it equals to the opposing viscous resistive forces and the particles reach their terminal settling velocity and eventually settles in the respiratory tract.

The third main mechanism of deposition in the respiratory tract is Brownian diffusion which is caused by collision of particles with gas molecules. When particle diameter comes close to the mean free path of the gas molecules and particle no longer moves as a continuum of gas. Under laminar flow conditions, a particle who touches the wall is absorbed and removed from the flow.

Other deposition mechanisms are turbulent flow regimes which is usually associated with Reynolds number (flow is laminar if Re < 2100, and turbulent if Re > 2100) The particles within the turbulent flow undergo changes in magnitude and direction which cause them to change their trajectories and eventually they deposit on the airway walls. [9]

Another deposition mechanism is electrostatic precipitation, which occurs by means of electrostatic charges can be a potential reason for deposition in the airway. In our case electrostatic precipitation is not considered as human airways are neutral. Interception. occurs when a particle comes very close to the airway wall that their edge touches the airway surface. The greater the length of the particle, the more likely the chance of the fiber touches the surface which causes retention in the airway.[9]

2.3   Particle Transportation

Airway geometry has a great impact on the flow field causing distinctive airflow patterns and therefore resulting particle deposition locations due to impaction, diffusion, or gravity. Airflow Pattern through the respiratory system is driven by the pressure difference from one end to the other. These inhalation and exhalation have a significant impact on fluid-particle dynamics. Other factors including particle size, shape, density, hygroscopicity, and surface properties have a major impact on particle transport, which determines its potential mechanism

of deposition. Moreover, the particle interaction with each other and with the cells and tissues of the respiratory tract also influences their transport. In complex flow regimes, particle-particle interaction, and particle-wall interaction must be considered which helps to predict the trajectories of the fiber particles [9][11] [10]

2.4   Particle Toxicology

Airborne particles, when inhaled are dangerous due to their deeper migration into lungs and can cross biological barriers to affect cells and tissues which are normally protected by layers. Furthermore, not only size but also their shape plays a vital role in deciding their uniform or nonuniform deposition. The non uniformity in the deposition pattern can cause even adverse effects on human health because they scattered around in airways. [10]

Fibers are widely used in industries due to their low cost and highly desirable physical and chemical properties. However, they are associated with potential health hazards when they are inhaled and deposited in the human respiratory system. For example, glass wool fibers in cigarette filters have been found lodged in the soft tissue of the deeper lung, which may develop tumors and cancerous cells. [10]

Several serious lungs diseases are caused by fiber inhalation such as malignancies (bronchogenic carcinoma and mesothelioma) and pulmonary fibrosis can be induced by inhalation of asbestos fibers. Several types of cancers such as lung cancer, laryngeal cancer, and pharyngeal cancer, are related to inhalation of fiber particles. [10]

2.5   Therapeutic Impacts

The respiratory system is becoming a more popular drug delivery avenue to combat various diseases. Targeted drug delivery has been and yet a great challenge for pharmaceutical companies in the field of pulmonary drug delivery, they confront problems in control release of drugs in pulmonary region. Inhalation drug mechanism (breathing into human lungs) is one of the important mechanisms along with other conventional drug delivery mechanisms such as oral (pill swallowing) and intravenous (injecting drugs into the veins). [10]

For pulmonary drug delivery, deposition pattern and clearance in the airway are two important aspects. As we have discussed above, the shape (fiber particle ratio 3:1, etc.) of the particles has an impact on their trajectories and deposition. Therefore, dimensional parameters of the particle have a great impact on optimizing the performance of drug delivery in comparison with spherical particles. The fiber particles are more likely to reach deep into lungs and have internalization ability, therefore it is promising that shape factor can increase the drug delivery performance. [10]

The development of pulmonary drug depends upon the dosimetry, safety, and efficacy of the drug. Other critical factors include low deposition fractions in the upper airway so that they can travel deep into lungs and to targeted areas of the pulmonary region. To enhance the efficiency of the pulmonary drugs, the particles parameters such as size, shape and surface properties are necessary. To identify the exact location of the particles to be deposited in the pulmonary region, calculation of the airflow in the selected lungs geometry using computational fluid dynamics (CFD) is needed. [10]

2.6   Numerical Investigation of Non-Spherical Particles

Fibers are particles with ratio 3:1 that means their length is bigger than their diameter and numerous studies demonstrated that they possess aerodynamics behaviour which is different than that of spherical particles due to their dimensional parameters resulting rotations during their motion. Therefore, it is important to accurately describe their orientation effect caused by their rotations. [8] [10]

2.6.1. Complete Numerical Simulation (CNS) / Direct Numerical Simulation (DNS)

Computational simulations of non-spherical particles have emerged as a major research tool over the past 20 years. So, does the numerous techniques of evaluating the behaviour of non-spherical particles have come into being such as Complete Numerical Simulation method (CNS), Direct Numerical Simulation method. To avoid confusion CNS and DNS are equivalent to each other and focuses on applying Navier–Stokes equations are applied to finite-size particles instead

of introducing "point particle" forces and able to produce accurate results of arbitrary shape particles. [22] [10]

2.6.2. Arbitrary Lagrangian Eulerian Technique (ALE)

Arbitrary Lagrangian Eulerian Technique (ALE) is used to solve particle motions in 2D, and 3D flow fields and it can handle particles of different sizes, shapes, and materials. ALE uses a technique based on a combined formulation of the fluid and particle momentum equations, together with a moving, unstructured, finite-element mesh technique to deal with the movement of the particles. The hydrodynamics forces acting on the solid particles are directly computed from the fluid flow field, where the motion of the fluid flow and solid particle trajectories are carefully coupled. The ALE method is also categorized as a boundary-fitted method. [10] [23]

2.6.3. Distributed Lagrangian Multiplier (DLM) Method

The Distributed Lagrangian Multiplier (DLM) method is based on the fictitious-domain method. The fictitious domain is derived from the idea that fluid fills the space inside of the particles as well as outside. Since fluid fills the whole flow domain, including particle volumes, a simple fixed finite element mesh can be generated to solve for the velocities of the fluid and the particles. As the mesh does not need to be refreshed in every time step, it is much more efficient when compared to the ALE method. The particle is tracked by using boundary control points that are on the particle boundary and move with the particle. [10]

2.6.4. Euler-Lagrange (E – L) Method

The E – L method is also called discrete phase model (DPMs), which provides a direct description of the particulate flow by tracking the motion of the individual particles. To calculate deposition and transportation, this method can be employed in two ways. [10]

2.6.4.1.   Effective Diameter Method

In this method non spherical particles are considered spherical with a parameter equivalent diameter. This phenomenon also addressed with different names such as Stokes equivalent diameter, aerodynamics diameter or the equal volume diameter. This method is a quick approximate analysis of non-spherical particle transport and deposition, if a proper

effective/equivalent diameter is employed along with hydrodynamics forces such as drag coefficient and lift coefficient. [10]

2.6.4.2.   Euler-Lagrangian with Euler Rotational Equation (EL – ER) Method

EL-ER method is employed by Euler Lagrange method, in which lagrangian function is constructed based on the kinetic and potential energy of the particle. This method combines the Euler Lagrange equation with Euler Rotational equation which describes both translational and rotational motion of the particle. [10]

2.6.5. Two Fluid Euler-Euler Method

The Two Fluid E-E Method solves two sets of algebraic conservation equations such as conservation of mass, energy, and momentum, for two different fluids simultaneously. In this technique both phases are treated as separate continua, both fluids can be different in density, viscosity, and other physical properties. Volume of Fluid (VOF) and Homogeneous Mixture model are the widely used models of the Two Fluid E-E Method. However, the method can also be computationally intensive and requires careful validation and calibration of the closure relations to ensure accurate results. [10]

2.6.6. Computational Fluid Dynamics – Discrete Element Method (CFD – DEM)

CFD-DEM Method is also called Combined Continuum and Discrete Model (CCDM). This method is used to compute the stresses and displacements in a volume containing many particles and is mainly used for modelling of fluidized beds and granular flows. [10]

This approach is a Lagrangian–Eulerian modeling of the multiphase fluidized medium in which a direct numerical integration of the individual particle trajectories is coupled to a continuum integration of the Navier–Stokes equation of fluid motion via an interphase interaction term. CFD-DEM Method is more accurate than any other under sever conditions such as intense particle collision. [10]

2.6.7. Tran Cong Approach (T – C Model)

Tran Cong et al. developed a new and accurate empirical correlation for the drag coefficient, C_D, of variously shaped particles while performing steady state free fall investigation of various particles of different geometrical shapes. The developed correlation depends upon the Reynolds number (Re) based on the particle nominal diameter, the ratio of the surface equivalent sphere to the nominal diameter (d_A / d_n), and the circularity (c). he conducted the experiment in a water- glycerin tank. Through this investigation he determined the terminal velocity of the irregular shape particles and the calculation of the drag force exerted on them. The particles used in this experiment are made with smooth glass spheres glued together and made up six different shapes (such as spherical, pyramidal, star shaped etc.). He concluded, at a given Reynolds number, the values of the drag coefficient for all the irregular particles were higher than the ones for spheres, regardless of the shape of the agglomerate. [36]

The most widely used empirical equation is Schiller and Naumann's correlation which is accurate for spherical particles. Tran Cong's approach is helpful in our investigation because it has a tendency to evaluate the asymmetrical shape of the particles.

2.7 Experimental Evidence of Fiber Deposition and Transportation

Haris and Fraser et al. have proposed an in-vitro model of these fiber particles with subject to fiber deposition in the respiratory tract and investigated aerodynamic behavior of thin straight rods like fibers. They predicted deposition values for rods of various equivalent aerodynamic diameters and lengths, for each of three tidal volumes and for each of three respiratory system compartments are reported [12] [10].

Myojo et al. investigated on the 3rd generation model of lung bifurcation with dimensions based on the symmetric model A of Weibel was designed to study lung deposition of fibrous aerosols. In this research he categorized the length of fibers in three classifications i.e., 10–20 μm, 20–40 μm, and 40–80 μm, by using steady inspiratory flow. He investigated glass fiber deposition on the daughter tubes and penetration of particles in the tubes were observed by means of scanning electron microscopy (SEM). With reference to Haris and Fraser's theoretical

values, he concluded that the deposited fraction is increased with an increase in fiber's length, but deposited fractions had much smaller values than their calculated results for each fiber length [13]. Later he also experimented with the total deposited fractions of fibrous aerosol on 4th generation model of lung bifurcation.[15]. Myojo et al. has also presented the deposition efficiency and deposition patterns experimentally in a in a human airway replica made from an adult cadaver. The replica includes the oral cavity, pharynx, larynx, trachea, and four generations of bronchi. This time he experimented with nine different sizes of monodispersed polystyrene latex fluorescent particles in the size range of 0.93–30 μm were delivered into the lung cast with the flow rates of 15, 30, and 60 l min^{-1} [14] [10].

The first experimental paper that systematically analyzed the deposition efficiency of asbestos fibers in a human lung-airway replica is that of Sussman et al. Sussman et al. investigated the effects of fiber diameter and length i.e., 1.5 μm − 2.5 μm, with flow rates co corresponding to cyclic inspiratory flow rates of 15 and 60 liters per minute (l/min). he identified deposition hot spots such as the posterior wall of the upper trachea and the airway bifurcations. He concluded, deposition efficiency generally increased with increasing flow rate and fiber length. The deposition efficiencies were greater at the bifurcations than along the airways. The ratio of deposition at the bifurcations to the rest of the airway was larger at flow rate 15 l/min than at 60 l/min for each generation [16] [10]

Su and Cheng as well as Zhou et al. experimentally investigated the deposition characteristics of different types of fiber material (i.e., CNTs, TiO$_2$, and glass) in two casts of human respiratory systems from mouth to lung airway generation 5. Su and Cheng reported that fibers with lower inertia are more likely to be transported to deeper lung airways, while fibers with higher inertia are more likely to be deposited at the oropharynx wall due to impaction. Moreover, Su and Cheng stated that the fiber deposition efficiency was generally lower than that of spherical particles. [17] [18] [19] [10]

Lizal et al. and his team developed a realistic human airway model and performed an experiment with glass fibers, in the seventh generation of branching to estimate the effect of fiber size and breathing pattern on fiber deposition. They extracted deposited fibers and rinsed them off from the model segments and gathered them on nitrocellulose filters. With the help of phase-

contrast microscopy and high-resolution camera was used to capture images of filters with fibers. New software was developed for automated image analysis and local deposition characteristics were calculated afterwards. They calculated the deposited efficiency and compared it to the data of spherical particles and noted that low deposition of fibers is due to their tendency to direct and align themselves in the flow direction. [20] [21]

2.8 CFD Evidence of Fiber Deposition and Transportation

The behaviour of these airborne fiberous particles can also be studied in-silico based experiments. Many researchers have proposed CFD Numerical Simulations to investigate fiber deposition and transportation behaviour of these particles in the human respiratory system.

The accuracy of deposition and transport of aerosols particles in the human respiratory system is a critical task in aerosol drug delivery, more specifically in inhalation products. The behaviour of these particles will determine whether to establish in vitro-in vivo correlation (IVIVC) or not, a complete understanding of the flow of aerosols at microscopic level is required. This task can only be done using CFD simulations in silico modelling which treats aerosol delivery as a two-phase flow. More specifically, CFD modelling couple with discrete phase model (DPM) and discrete element method (DEM) approaches. Fen et al. presented research in which he explained recent developments in this area such as geometry models of the respiratory tract, CFD turbulence models for gas phase and its coupling with DPM, DEM for aerosols and CFD investigations on geometric variations, flow, and powder characteristics. His review stated that CFD models successfully evaluated and predicted the aerosols deposition pattern in human respiratory tract. [27]

Most of the particles encountered in engineering practices are not 100% spherical, they are irregular in shape, their shape plays a key role in determining their behaviour. Zhong et al. presented the research in which he investigated DEM is a promising approach to model non spherical particulate system (NSPS) and explain that DEM non spherical model has the capability to couple with CFD for particle fluid flow. [30]

Chen et al. employed CFD-DEM approach to predict the behaviour of the gas-solid flow with strong coupling and the motion of non-spherical particles and achieved desired results with

great potential of deposition and transportation in the pulmonary region. He used an idealized pulmonary airway model of generation 3 to 5 which has the same geometric parameters that has been previously used by Kim and Fisher et al. By examining the particle positions at various time intervals, The findings indicate that a particle's initial position would have a significant impact on its course. When the near wall particles cross the airway, they disperse uniformly in the daughter tubes. The inner side tubes of generation 5 carry the model's most centered particles. As the distance between a particle's initial position and the tube center grows, the trajectories of other particles would switch from the inside tubes to the lateral ones of the previous generation. [24]

Tao et al. used CFD-DEM approach, he modelled ellipsoidal particles by overlapping three spheres and simulated the flow in the hopper. He considered the contact forces and gravity while considering wall normal pressure and velocity distribution during the flow. He concluded; that the wall normal pressure for two kinds of particles has a peak value at the transition from the vertical section to the slope wall. The horizontal pressure distribution always fluctuation and the pressure at edges is a little higher than in the center. The velocity of ellipsoidal particles is smaller than that of spherical particles.[25]

Cheng et al. presented a V shaped pleated air filter media and used CFD-DEM method to simulate the deposition. He investigated that CFD-DEM method can effectively applied to the macro research of pleated air filter media, and particles will form dust layer and dendrite structure on the fiber surface, and the dust layer will affect the subsequent air flow organization, and the dendrite structure will eventually form a "particle wall". The formation of the "particle wall" will prevent the particles from moving further in the fluid domain, which makes area of pleated angle become the "low efficiency" part about the particle deposition. Compared with area of pleated angle, the particles are concentrated in the opening area and the middle area of the pleated to agglomerate and deposit. [26]

Morteza et al. investigated fibrous particle transportation and deposition by unsteady airflow in the human upper airways during the breathing cycle with the help of CFD method. He anatomically realistic model of airway passage including vestibule to the end of the trachea was constructed from the CT images of a 24-year-old healthy woman. In his research, user-defined

functions (UDFs) are employed with discrete phase model (DPM) in Ansys Fluent and used ellipsoidal particles motion in transient airflow. The developed UDF was used to solve the coupled translational and rotational equations of motion of ellipsoidal fibers and to analyze their dispersion and deposition in the upper airways. The presented results showed that the steady simulation with an appropriate equivalent airflow rate can predict the total fibrous particle deposition during cyclic breathing with reasonable accuracy. [28]

Van et al. presented a complete framework to predict the behavior of interacting non-spherical particles with large Strokes numbers in turbulent flow. He summarized rigid particle dynamics such as particle to particle collision by modeling a particle-rough wall interaction model and explained the collision between non-spherical particles. he achieved this task by using the framework coupled with a DNS-LES approach to simulate the behaviour of horizontal turbulent channel flow with 5 differently shaped particles: a sphere, two types of ellipsoids, a disc, and fibre. The drag and lift forces and the torque on the particles are computed from correlations which are derived using true DNS. [29]

The simulation results demonstrate that non-spherical particles typically position their longest axis perpendicular to the local flow direction to locally maximize the drag force. This phenomenon is further elucidated by resolving direct numerical simulations of an ellipsoid in a flow. His simulations demonstrate that if a non-spherical particle's axis is not aligned with the flow, the high-pressure region on the acute sides of the non-spherical particle results in torque. Only when the particle's axis is parallel to the local flow direction then this torque becomes zero. Furthermore, he concluded that the longest axis should be perpendicular to the flow for the particle to be at its most stable. [29]

3. Analysis of Tools

3.1 Simcenter STAR CCM+

Simcenter CCM+ is developed by Siemens Digital Industries. It is used to simulate and analyze the behavior of fluid flows and wide range of complex single-phase flows (such as steady state and transient, laminar, and turbulent flows, compressible and incompressible) as well as multi-phase flows.

Simcenter STAR CCM+ can also model complex multiphase flows (such as liquid-gas, liquid-liquid, solid-liquid and solid-gas flows) with intense multi-phase modelling techniques (i.e., the Volume of Fluid (VOF) method, the Eulerian-Lagrangian method, and the Eulerian-Eulerian method etc.) and able to visualize simulation results, streamlines and contour plots.

3.2 Computational Fluid Dynamics (CFD)

CFD in Simcenter STAR CCM+ is proven to be an accurate tool for multiphase flows, especially when a fluid phase contains another phase such as solid particles phase. In this type of CFD simulation fluid phase is modeled using lagrangian approach (LA) defines what particles to enter the domain and particle phase is modelled using DEM technique to simulate the behaviour of particles and their interaction with other particles and within the fluid phase. In Simcenter STAR CCM+, particles enter the fluid continuum through injectors. The injector defines where, in what direction, and with what frequency, the particles enter.

This kind of flow regime is called lagrangian multiphase (LMP) and deals with variety of flow processes either it is a disperse phase or continuous phase. However, for the flow if it is dealing with small number of disperse phases, it is possible to solve the governing equation for every particle whereas for large number of disperse phase, a statistical approach is more practical, hence small number of computational parcels represents the total population of dispersed phases. Each parcel represents a localized group of disperse phase having the same properties. The representation of parcel and the particle is shown in fig 4. [34]
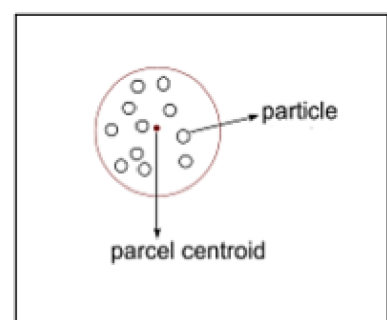
Figure 4: representation of a parcel vs particle [34]

The lagrangian multiphase (LMP) is also compatible with time models. In steady condition, the approach is categorized as a trajectory method, in which it records the tracks of the parcel and the variations of the state (state means velocity, temperature etc.). Each track records the complete lifetime of one parcel, information regarding when it is injected and when it left the domain, as shown in fig 5. [35]
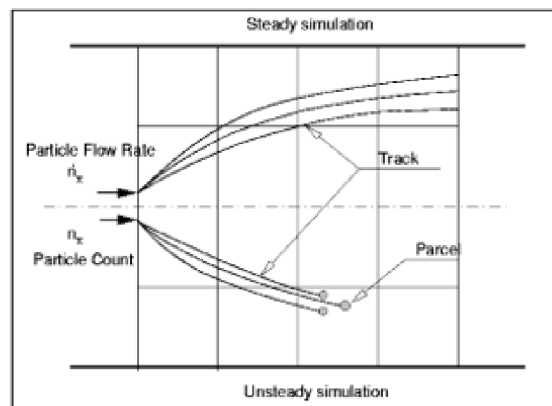

Figure 5: different b/w steady and unsteady simulation and Particle tacking over time. [35]

In lagrangian multiphase unsteady conditions, the Discrete Element Method (DEM) adds more details in terms of contact forces. In this flow condition, it provides the solution at the given instant in time and its state (such as position, velocity, and temperature) of each parcel. The tracking of parcels can be visualized by streamlines in post processing. [35]

Particle in the CFD-DEM simulation is assigned a set of physical properties such as mass, shape, and material properties. The forces acting on each particle are calculated based on the inter-particle interactions and the external forces applied to the phase. The positions, velocities, and orientations of the particles are then updated in discrete time steps to simulate the motion of the particle.

3.2.1. Euler-Euler Method (E – E Method)

Euler–Euler (E –E) model describes both the fluid and the particulate phase often referred to as two phase simulation in which liquids are treated as interpenetrating continua. The most distinctive feature in this method, that particles are not tracked in space and time. Instead, their

phase properties (e.g., speed, size, composition, etc.) are considered. The phases in Eulerian framework can be gas, liquid, or solid particles. Each phase has its own energy, velocity, and other physical parameters as well as interactions can also be modified between phases. [37]

3.2.2. Discrete Element Method (DEM)

DEM model is an extension of lagrangian framework, to simulate the motion of many interacting discrete solid particles, this method is usually used for granular flows. DEM in Star-CCM+ requires powerful simulation setups so that they can be applied to the region with and without volume mesh. The distinctive feature of the DEM is that they can calculate inter-particle contact forces which cannot be ignored in terms of loaded and dense flows. [38]

Another important feature which cannot be missed is that DEM is based on soft particle formulation where particles are allowed to develop an overlap. This method also allows to alter particle material and geometric properties. [38]

3.2.3. Lagrangian Framework with Modified Drag Coefficient

In the Lagrangian framework, which is commonly used in particle dynamics, the motion of individual particles is described based on their positions and velocities. The concept of drag coefficient may not be applied directly, however there are two drag models that can propose an authentic solution to this problem.

3.2.3.1   Tran Cong Drag Model

The Tran Cong method is one of the suitable options in this investigation because the Tran Cong approach cooperates with asymmetric particles and its empirical formulation of drag coefficient can be able to modify the drag coefficient for asymmetric particles. [36]

One of the approaches is used in this method is to obtain the shape factor in terms of volume-equivalent -sphere diameter or nominal diameter d_n and is given by, [36]

$$d_n = \sqrt[3]{\frac{6V}{\pi}} \qquad (1)$$

Where V is the particle volume. Another similar parameter in terms of projected area of the sphere A_P which is referred in the surface-equivalent-sphere diameter d_A and is given by, [36]

$$d_A = \sqrt{\frac{4A_P}{\pi}} \tag{2}$$

By evaluating eq (1) and (2), the ratio $\frac{d_n}{d_A}$ can be used in terms of drag coefficient. In similar manner, particle elongation can also be taken into account by describing their aspect ratio which is denoted by β and is given by, [36]

$$\beta = \frac{4\left(\frac{d_n}{d_A}\right)^3}{\pi} \tag{3}$$

Another important approach in determination of shape factor is the particle sphericity (φ). It is a ratio if surface area of the equivalent-volume-sphere to the actual surface area of the particle A, and is given by, [36]

$$\varphi = \frac{\pi d_n^2}{A} \tag{4}$$

The sphericity (φ) is dimensionless number for characterizing the shape of isometric irregular particles. however, in some cases sphericity (φ) is difficult to measure due to the surface area of the irregular particles. Hence why shape factor comes into consideration and is given by, [36]

$$c = \frac{\pi d_A}{P_P} \tag{5}$$

Where P_P is the projected area of the particle in the direction of motion. However, to determine the state of drag force, drag coefficient can be modified by using an approach in which projected area of an equivalent-volume sphere, where particles nominal diameter d_n plays an important role. The 2nd important approach by considering the particles actual projected surface area of the irregular particle. Hence the drag coefficient C_D is given by, [36]

$$C_{DA} = \frac{4}{3} \frac{d_n^3}{d_A^2} \frac{(\rho_s \rho_f)}{\rho_f} \frac{g}{w_s^2} \qquad (6)$$

3.2.3.2 Haider and Levenspiel Drag Model

The "Haider and Levenspiel" approach is a method which is used to estimate the drag coefficient for solid particles which are moving through fluid medium. The method is particularly useful for predicting the drag coefficient for non-spherical particles by taking Reynolds number, aspect ratio and particle orientation into account.

The formulation presented by "Haider and Levenspiel" which considers the shape factor (c) of the particle (sphericity is a ratio of the surface area of the volume-equivalent-sphere) eq (7), based on this approach the drag coefficient C_D eq (8) is modified. [57]

$$c = \frac{\pi d_A}{P_P} \qquad (7)$$

$$C_D = \frac{24}{Re} r \left[1 + \frac{0.15}{\sqrt{c}} (r\, Re)^{0.687} \right] + \frac{0.42 r^2}{\sqrt{c}[1 + 42500(r\, Re)^{-1.16}]} \qquad (8)$$

Therefore, in this "Haider and Levenspiel" (H − L model), most of the empirical formulation is taken from Tran Cong (Tran Cong et al), usually it is called T − C model. Hence, in T − C model, particle shape factor (c) and the ratio of surface-equivalent diameter to the volume-equivalent diameter ($r = \frac{d_A}{d_{Ps}}$) are taken into consideration to modify the drag coefficient C_D. [57]

4. Numerical Simulation

Several scientists have studied the morphology of the respiratory airway geometry, because of its structural complexity and concluded that most of the models cannot predict the realistic particle deposition patterns. However, recent developments in computed tomography (CT) and magnetic resonance imaging (MRI) have provided an opportunity to reconstruct the respiratory airway tree with all its anatomical complexities. These realistic airway models have been used for decades in computational fluid dynamics (CFD) and experimental investigations of particle transport and deposition in the respiratory system. [31]
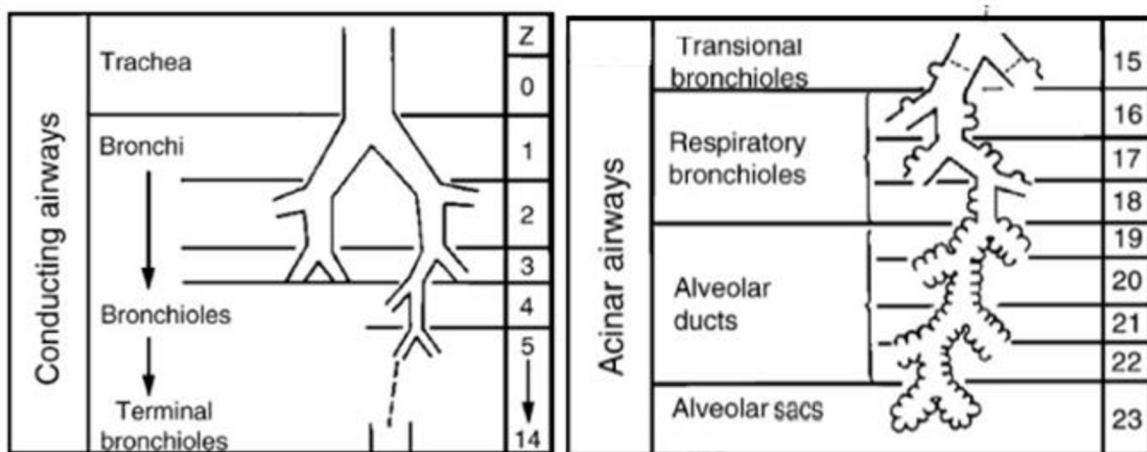
Figure 6: schematic of the branching airways in Weibel's model. Source [31]

The most well-known proposed geometry is Weibel's model, which is simple and symmetric (Weibel et al. 1963). Presentation of this model was one of the first steps in development of idealized respiratory airway models and it was used in several different numerical and experimental studies The human respiratory system has several sections, and the tracheobronchial region is one of them. According to Weibel's model, there are 23 generations of bifurcations, It looks like an upside-down tree, where the thickness and diameter of branches get thinner and thinner with every branching step as shown in fig. 6.
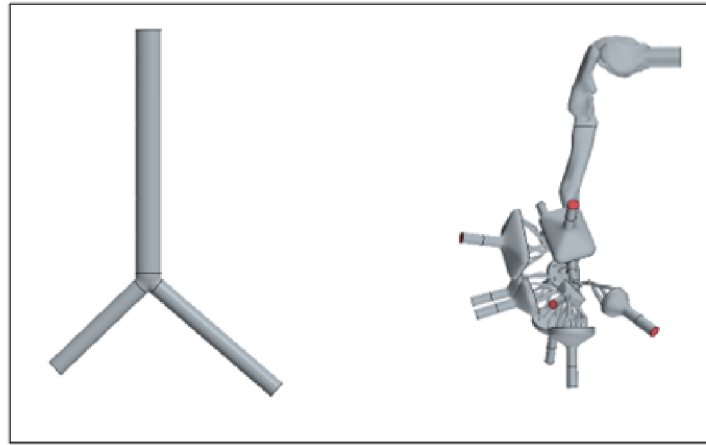
Figure 7: Y Model geometry (left) and a model of human lungs geometry (right) [40]

Although there are several variations in geometries available to perform this investigation, the geometries we are using in this study are shown in fig. 7. In the Y–model geometry shown in fig. 7 (left), DEM approach is analyzed and in the model geometry of human lungs shown in fig. 7 (right) modified T – C drag model is employed. The results of deposition fraction of fiber particles are then analyzed. [31]

4.1 Y Model Simulation

4.1.1 Geometry

Geometry is created based on the parameters given in Lizal's experimental study. The

angle of bifurcation and the dimension of the geometry is shown in fig. 8. [4]
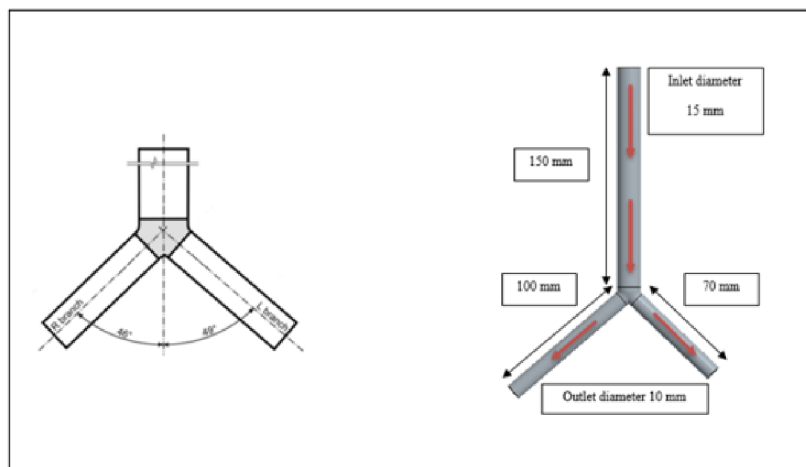
Figure 8: Visualization of Y model geometry and its dimensions. [4]

4.1.2 Meshing

To generate mesh, we have selected a polyhedral masher because of its balanced solution to complex mesh problems. Polyhedral mesh is relatively easy to build, it contains approximately 5 times fewer cells than tetrahedral mesh as well as it allows multi region meshes with a conformal mesh interface. The mesh contour can be seen in fig. 9.
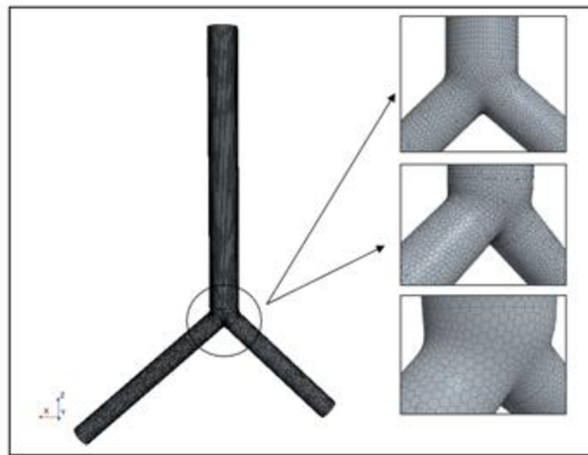

*Figure 9: Polyhedral mesh of the Y model geometry*

The size of the average element is 0.001 m. Over 2 hundred thousand cells were generated; details are shown in tab. 2 shows the total number of generated cells, faces and vertices. The prism layer mesh model is used with core volume mesh to generate orthogonal prismatic cell layer next to wall surface to better describe the area of boundary layer. The thickness of prism layer is 0.001 m.

Table 2: number of cells, faces and vertices of the Y model geometry.

Cells	245241
Faces	1123398
Vertices	709905

No. of Prism Layer	10
Base Size	0.001 m = 1.0 mm
Prism layer thickness (next to wall)	$1.0 \quad .10^{-6}$

This layer is helpful to improve accuracy and it is dependent upon thickness, number of layers and size distribution as shown in fig. 10.
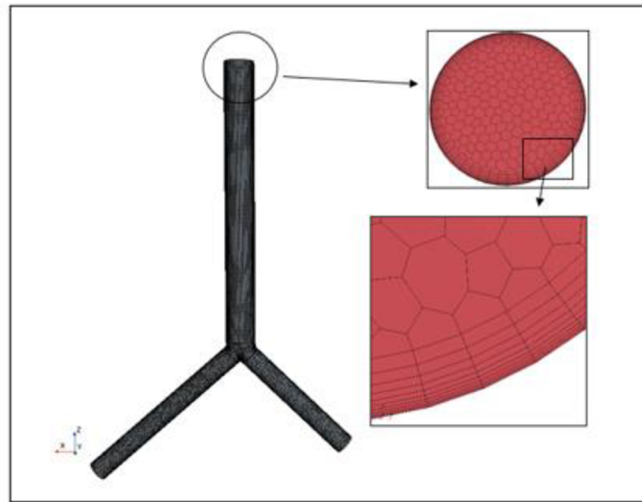

Figure 10: visualization of prism layer, number of prism layers are 10 (ten layers)

Surface masher is another tool to improve the overall quality of the initial mesh and it is usually used as initial mesh from which volume cells are generated towards the interior of the domain. The main purpose of this tool is to retain the geometric features by preserving the edges which provides better representation and projections of the CAD geometry, this is because a conventional polyhedral mesh created by CFD software is unable to use for CFD purposes. Therefore, it needs to be re-meshed in CFD and only then can be used as basement for volumetric mesh.

4.1.3 Physics Setup

The physics model is the physical phenomenon in a continuum which represents primary variables of the simulation. The gas is set to "Air" with density and dynamic viscosity 1.18415

kg/m^3, 1.85508 .10^{-5} Pa-s respectively. The flow condition is set to mass flow rate 0.072 kg/s. To inject particles in the flow, we set up initial flow condition, the flow is solved with steady regime to obtain initial condition of velocity fields, one step second of unsteady phenomenon was calculated and after that the multiphase model with DEM approach was enabled onto the fully developed airflow.
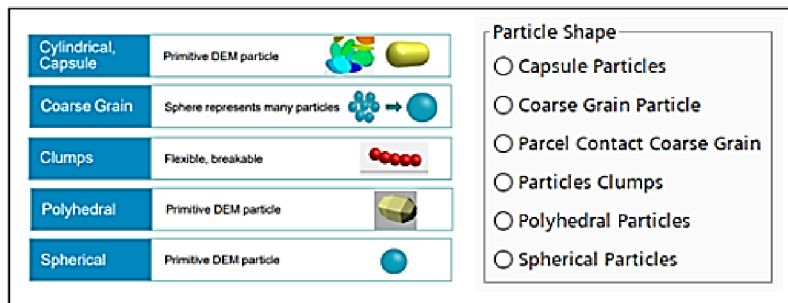

Figure 11: different kinds of DEM particles [43]

DEM lagrangian phase allows us to choose multiple types of particles including spherical particles coarse grain particles, composite particles, and particle clumps model etc. Their evaluation is added in tab 3.

Table 3: Evaluation of DEM particles.

Spherical Particles	The Spherical Particles model uses a single sphere to represent a particle
Coarse Grain Particle	Many particles are joined together to form a particle parcel and contact forces consider each parcel a single large particle.
Composite Particles Model	Multiple spherical particles combined to form a non-spherical particle; spheres have non-breakable bond between them during simulation. This model treats the individual sphere as a separate entity so their contact between them resolved separately.
Particle Clump Model	Multiple spherical particles can be bonded together to represent a non-spherical particle & their assemble can be defined in the shape editor. Their bond can be evaluated by phase interaction model, each sphere is treated as an individual particle and their connected through parallel

	bonds. This bond can be modeled as breakable bond with "simple failure" model or "constant rate damage" model. When it breaks the particle interact according to "Hertz Mindlin" law instead of parallel bond.
Polyhedral Particles	This model includes the particles of any polyhedral shape rather than particles composed of combination of spheres.
Cylindrical Particles	Model includes to use cylindrical particles of specified size and proportion rather than particles composed of combination of spheres.

In our investigation, we have selected particle clumps model and shown in fig 12. The particles are glued together to form a particle clump model, the number of spheres that are joined together is 10. The aspect ratio is β = 10 and the nominal diameter of each sphere is 3.8 μm.
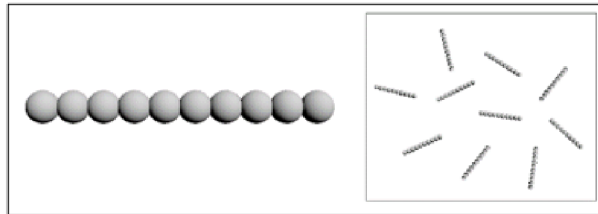
Figure 12: particle clump model (10 Spherical particles are glued together)

To calculate the volume and aerodynamic diameter of the particle clump, the following formula is used, and details of the parameters acquired are shown in tab. 4.

$$V = \frac{4}{3}\pi r^3 \tag{9}$$

Table 4: Aerodynamic diameter of the particle clump

Radius of the sphere	0.0000019 m

|	
Volume of the sphere	$2.8 \cdot 10^{-17}$ m^3
Aspect ratio	10
Volume of the particle clump	$2.87 \cdot 10^{-16}$ m^3
Aerodynamic radius of the particle clump	$4.09 \cdot 10^{-06}$ m
Aerodynamic diameter of the particle clump	$8.18 \cdot 10^{-6}$ m

The particles are solid glass particles with density, poisson's ratio and young's modulus 2500 kg/m^3, 0.235 and $7.58 \cdot 10^{-10}$ Pa, respectively. The gas phase is carrying the particle phase, particle-particle interaction and particle-wall interaction are specified with Hertz Mindlin contact models. [44] The contact model activated by default with particle clumps, such as bonded contact (determines the connection and inter-particle forces) and Hertz Mindlin (determines contact between particles) model whereas rolling resistance (determines method of calculation of constant torque, displacement damping or force proportionality) is an optional model in the phase interaction. The phase interaction used in our simulation for both phases are shown in fig. 13. [45][46][47]

Figure 13: particle phase interaction (left), fluid phase interaction (right)

The particle is injected into the flow through the inlet with the help of a part injector. The injector is set up with 1 injector point. As established, particle is glass material with density 2500 kg/m^3, aerodynamic diameter 8.187 μm and aspect ratio 10. The simulation is set up for 1000 steps and 100,000 sub-steps with a 1st order tracking integration method. The Residual plot can be seen in fig. 14.
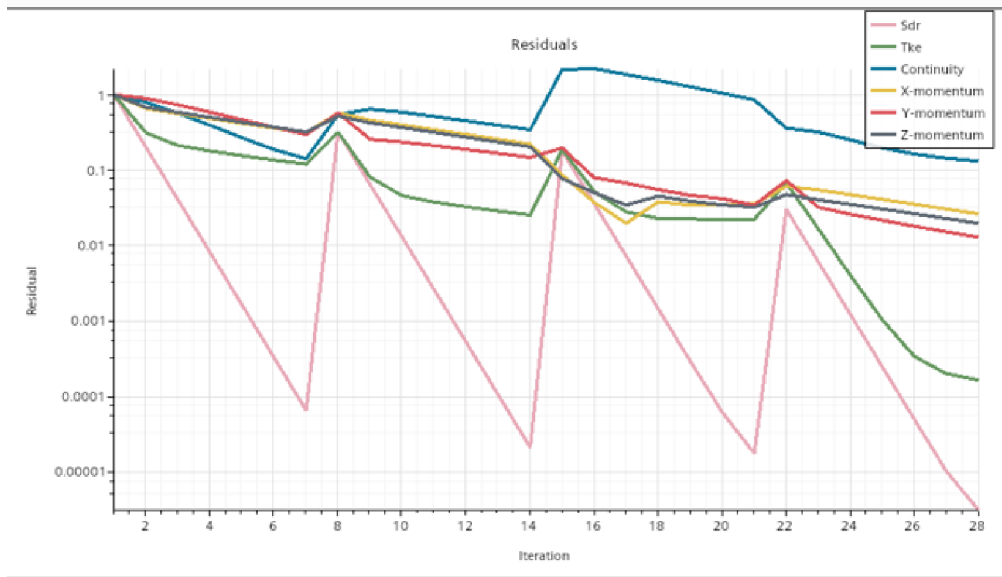
Figure 14: residual / convergence plot

4.2.4 Results

To validate the applicability of this simulation, it is concluded that this method of monitoring the particles is doable, but the time constraints make it undesirable. The particle clump model is used in this investigation with aerodynamic diameter of 8.187 μm which attains the velocity of 2.3 m/s during its motion, and DEM particle motion criteria states that particle cannot move $1/10^{th}$ of its radius and $1/10^{th}$ of its time step [59], then its track length would be $4.09 \cdot 10^{-07}$ hence we calculated the time step which is $1.77 \cdot 10^{-07}$.

The above parameters are used to calculate the real time of their motion in the Y model and their details are shown in tab. 5.

Table 5: DEM Particle time scale parameters

Velocity	2.3 m/s
Trajectory	0.25 m
Time	0.1 s
Time step	$1.77 \cdot 10^{-07}$

Iterations	610735
One Iteration	70 s
Time calculation	42751476 seconds
	712525 minutes
	11875 hours
	495 days

To sum up, DEM approach is a valid methodology to monitor the tracks, however, as shown in results, it takes enormously long time to compute the particle motion and makes it a unfavorable technique.

4.2 Model of Human Lungs Simulation

4.2.1 Geometry

The geometry used in this simulation is shown in fig. 15. This is generation 7 airway model of human lungs which is used in several aerosol transport and deposition research at Brno University of Technology. The tracheobronchial region of geometry is based on the reference model of Schmidt et al and detailed description of the airway geometry can be found in Lizal, Elcner, Hopke, Jedelsky, and Jicha (2012). [41][42] [40]
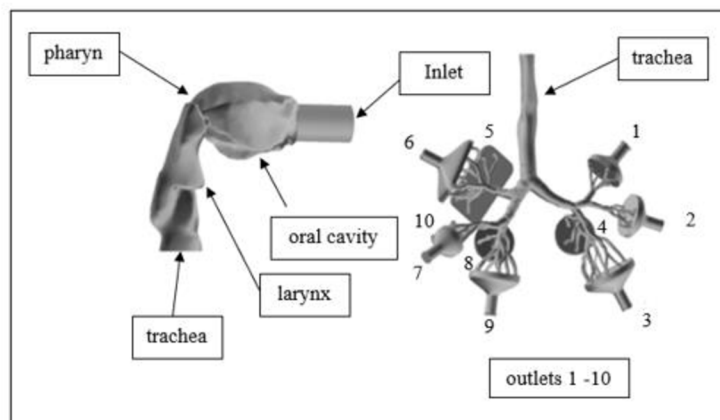

Figure 15: visualization of human lungs model, the vital parts of the geometry is labelled (for visualization oropharyngeal-laryngeal part is removed from the tracheobronchial region) [40]

The development of this geometry is described in the development research of Lizal et al. [60], and brief introduction to this, geometry consists of oral cavity, larynx, trachea, and bronchial tree to the seven-generation bronchial branching. The terminal branches of the bronchial tree are brought into ten (10) collectors which relate to breathing simulators by tubes during the research. The model is further divided into segments and specific numbering given to the specific regions as
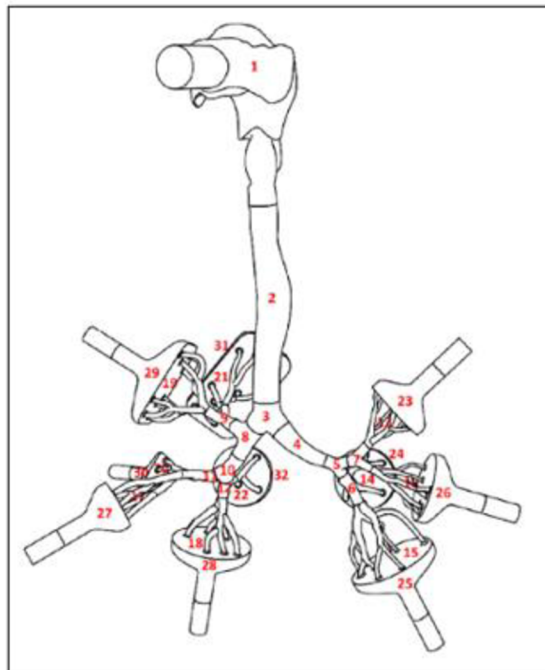
Figure 16: overview of the model segments and numbering of specific regions [61]

described in Lizal et al. [60], and is shown in fig. 16, and dimensions are shown in tab. 6.

Table 6: parameters of the geometry of the human lungs model [61]

Segment number	Generation of branching	Diameter	Surface of segment	Volume of segment
-	-	mm	cm^2	cm^3
1	0	20.0	174.73	74.41
2	0	16.3	60.3	8.31
3	0-1	14.7	9.72	3.02
4	1	10.2	9.27	0.77

5	1-2	7.0	3.66	0.64
6	2-3	5.5	5.61	0.64
7	2-3	6.0	3.82	0.38
8	1-2	12.1	8.63	1.1
9	2-3	7.8	5.81	0.69
10	2-3	8.5	4.92	0.5
11	3-4	6.5	4.75	0.52
12	3-4	7.0	3.89	0.42
13	3-6	3.0	9.4	0.64
14	3-6	3.3	15.19	0.93
15	3-7	3.3	23.99	1.8
16	3-7	2.5	9.36	0.38
17	4-7	3.6	13.63	0.83
18	4-7	4.1	16.79	1.44
19	3-7	3.6	20.53	1.62
20	4-6	2.6	5.41	0.25
21	3-6	3.4	19.68	1.42
22	4-7	3.4	9.82	0.66

4.2.2 Meshing

To generate computational mesh on this model, we used polyhedral meshing technique, complemented with prism layer mesher and surface mesher. Approximately 2.6 million cells were generated on the model, extended parameters are shown in tab 7 and the visualization of the meshing contour is shown in fig. 17. The size of the average element is 0.0015 m, this value is an approximation to discretize all

Figure 17: polyhedral mesh contour of the model geometry of human lungs

regions of the geometry even in regions with small branch diameters. The near wall region is treated with prism layer.

Table 7: overview of the parameters of the mesh

Parameters	Description
Base Size	0.0015 m = 1.5 mm
Prism Layer thickness	30 % of base size
Prism layer thickness next to wall	$5.0 \ .10^{-5}$
Number of Prism Layer	8
Cells	2606738
Faces	11485223
Vertices	7053794

4.2.3 Physics Setup

The numerical investigation will be compared with the previously performed investigations by Belka et al. [59] This investigation consists of two steps. The 1st step involves only the airflow inside the model and in 2nd step lagrangian multiphase model for particle.

The flow conditions are set to inspiratory flow with 15 L/min though inlet. Airflow inside the replica was solved as steady with a segregated model using 2nd-order upwind discretization scheme for convection. The density and viscosity of the medium (air) is set to 1.184 kg/m^3 and 1.85 .10^{-5} Pa-s. The glass fibers of size 3.39 .10^{-6} m, are used with particle density of 2500 kg/m^3. Turbulence was modelled using Reynolds Average Navier-Stokes equation (RANS) approach with two-equations viscosity SST $k - \omega$ model of turbulent conditions. Near-wall area was treated using low wall y+ treatment which fully solves velocity profile in boundary layer. For this approach it is necessary to comply with the condition of wall y+ value equal or below 1 at the boundary along which the medium flows. Simulation of airflow inside the model was solved for 5000 of iteration. All residuals (such as momentum, continuity, and turbulent variables) converge under threshold accuracy of 10^{-3}. The residual plot is shown in figure 18.
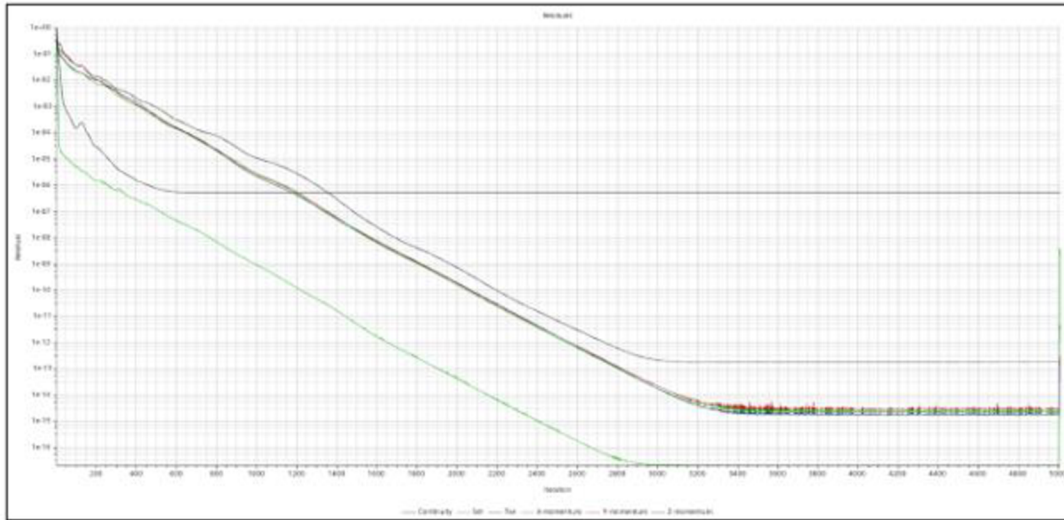
Figure 18: residual / convergence plot

The 2nd step is to model the lagrangian multiphase, spherical particles which react to drag force, pressure gradient and turbulent dispersion was enabled. This investigation involves lagrangian framework with modified drag force to track the particles within the airways. However, a specialized field function is modeled to calculate the aspect ratio of the particle, Reynolds number and the drag model. The drag coefficient of the drag force model was prescribed using field function according to T – C drag model as shown in tab 8.

Table 8: field function definition

	$$C_D = \frac{24}{Re}\, r\left[1 + \frac{0.15}{\sqrt{c}}(r\,Re)^{0.687}\right] + \frac{0.42r^2}{\sqrt{c}[1 + 42500(r\,Re)^{-1.16}]}$$
Field Function	```((24/${ParticleReynoldsNumber})*(pow(${Beta},(1/6)))) *((1+(0.15*(pow(${Beta},(1/4)))))*((pow((pow(${Beta},(1/6))*${ParticleReynoldsNumber}),0.687)))))+((0.42*(pow((pow(${Beta},(1/6)))),2))*(pow(${Beta},(1/4)))))/(1+42500*(pow((pow(${Beta},(1/6))*${ParticleReynoldsNumber}),-1.16))))```

The last step is to inject the particle into the flow through mouth cavity. The part injector is used to launch particles in the flow and set it up to 100 injector points. Each injector point is evenly distributed on the inlet of the mouth cavity as shown in fig. 19. The injector point was set to 1000 parcels for each injector point (total 100,000 glass particles of density 2500 kg/m^3 and aerodynamic diameter 3.39 E^{-6} m) with aerodynamic diameter of 3.4 μm and aspect ratio 18. (Belka et al.) [59]. The simulation is set up for maximum 20000 sub-steps and maximum residence time 100s with 2nd order tracking integration method. A total of 99,771 particles were deposited.
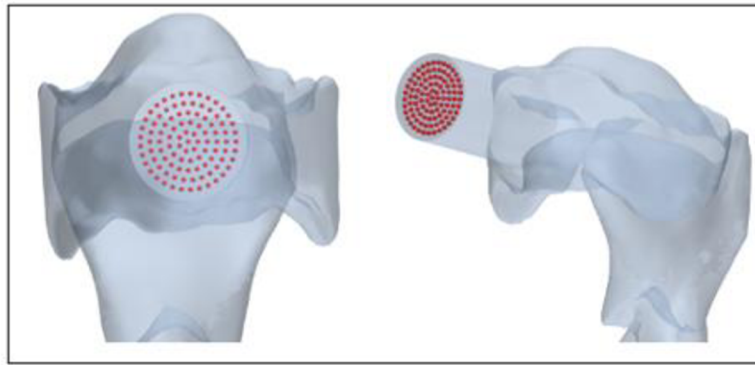
Figure 19: visualization of part injector on inlet (mouth entrance of the model)

4.2.4 Results

The fiber deposition is calculated in the various regions of the respiratory tract model with the help of equations below. The deposition of particles in terms of deposition fraction is denoted by (DF) and deposition efficiency (DE).

$$DF = \frac{number\ of\ deposited\ fibers\ in\ a\ specific\ segment}{number\ of\ fibers\ entereing\ the\ whole\ domain} \tag{9}$$
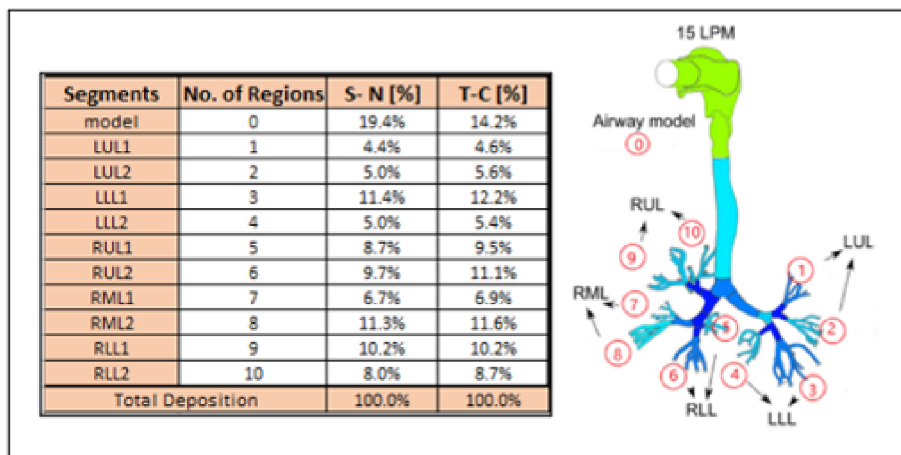
$$DE = \frac{number\ of\ deposited\ fibers\ in\ a\ specific\ region}{number\ of\ fibers\ entereing\ this\ (specific)\ region} \tag{10}$$

We have performed simulation computed by S − N model and T − C model and evaluated the deposition fraction in various regions of the model to compare spherical particles behaviour

and describe differences between fiber and spherical particle deposition. To read and understand result percentages, we have divided the model into different regions and segments fig. 20.

Based on these simulation results, the airway model (denoted by region 0) yielded deposition fraction 19.4% by S-N model and 14.2 % by T- C model. The tracheobronchial deposition fraction by S – N model at flowrate 15 (L/min) values 4.4% (at location LUL, denoted by 1), while 4.6% by T – C model at the same location. The detailed deposition at different regions and segments are shown in fig. 20. It is seen by deposition results that, values obtained by S – N model are consistently lower than the values achieved in T – C model. It could also be true the field function we used in the T – C model has modified Reynolds number for the particles used, that could be the reason for the high deposition fraction.

Segments	No. of Regions	S- N [%]	T-C [%]
model	0	19.4%	14.2%
LUL1	1	4.4%	4.6%
LUL2	2	5.0%	5.6%
LLL1	3	11.4%	12.2%
LLL2	4	5.0%	5.4%
RUL1	5	8.7%	9.5%
RUL2	6	9.7%	11.1%
RML1	7	6.7%	6.9%
RML2	8	11.3%	11.6%
RLL1	9	10.2%	10.2%
RLL2	10	8.0%	8.7%
Total Deposition		100.0%	100.0%

Figure 20: regional deposition fraction of flowrate 15 L/min [59]

The deposition fraction computed by both models is higher in oral airways and in trachea region (model, denoted by 0), whereas maximum local deposition fraction is seen in T-C drag model at segment LLL 1 (denoted by 3) in fig. 27.
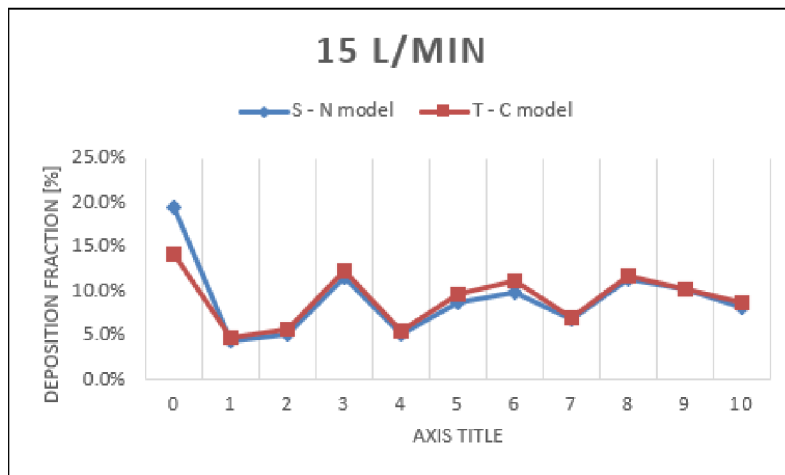
Figure 21: deposition fraction of particles, computed by S - N model vs. T - C model.

The distribution of deposition fraction is shown in plot in fig. 21. The changes can be observed in the oral and trachea region deposition with highest deposition fraction as well as a significant change between both drag models. On the other hand, local maximum at segment number 3, which is the region where the trachea transforms itself into two main bronchi (denoted by 3 in fig 22).
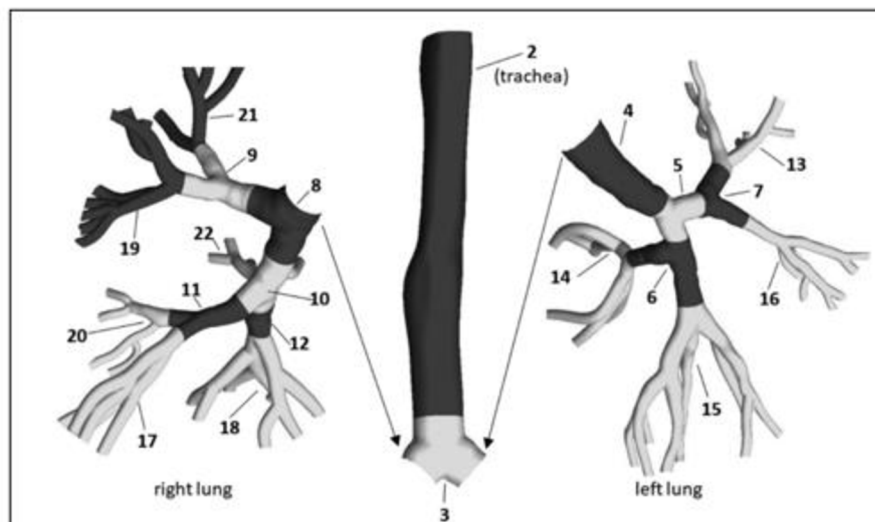

Figure 22: segmentation and numbering of the human lungs model (geometry is cut into three parts for better visualization.[57]

5. Results and Discussion

The extensive literature review shows there are 6 defined ways by which these particles can get trapped inside human lungs. The deposition phenomena include inertial impaction, sedimentation, Brownian, diffusion, electrostatic precipitation etc., some of these ways has least influence on deposition or neglected and has least affect, such as Brownian diffusion is mostly applicable on particles smaller than 0.1 micrometer and the particles used in this investigation is larger. The electrostatic precipitation is another neglected phenomenon in our investigation because there is no electrostatic charge in the particles. The main deposition mechanism we are dealing with is inertial impaction due to turbulent flow regime and sedimentation which is settlement due to gravity or the interaction of particle with the wall. [61]

The deposition fraction results of $S - N$ drag model and $T - C$ drag model is compared with Belka numerical investigation. Belka et al. (2018) [59]. Fig. 23 illustrates deposition percentages of flowrate 15 L/min, in $S - N$ drag model approach, $T - C$ drag model approach and Belka's approach.

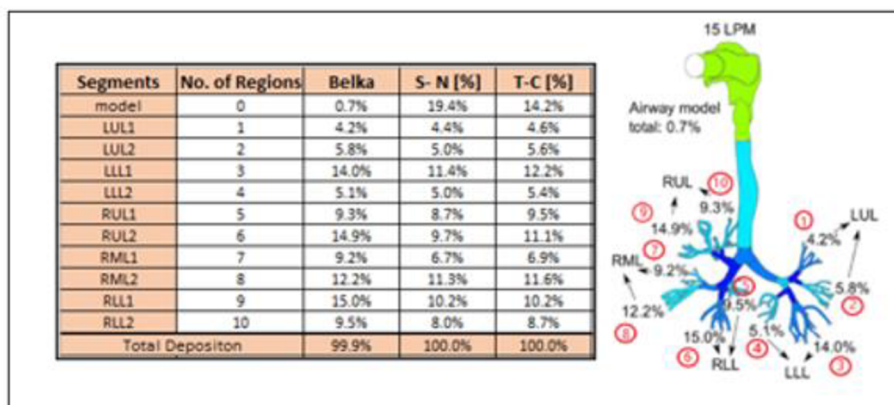| Segments	No. of Regions	Belka	S- N [%]	T-C [%]
model	0	0.7%	19.4%	14.2%
LUL1	1	4.2%	4.4%	4.6%
LUL2	2	5.8%	5.0%	5.6%
LLL1	3	14.0%	11.4%	12.2%
LLL2	4	5.1%	5.0%	5.4%
RUL1	5	9.3%	8.7%	9.5%
RUL2	6	14.9%	9.7%	11.1%
RML1	7	9.2%	6.7%	6.9%
RML2	8	12.2%	11.3%	11.6%
RLL1	9	15.0%	10.2%	10.2%
RLL2	10	9.5%	8.0%	8.7%
Total Depositon		99.9%	100.0%	100.0%

Figure 23: deposition fraction, Belka vs. S - N drag model vs. T - C drag model.

The deposition fraction in oropharyngeal-laryngeal region, achieved by $S - N$ and $T - C$ drag model is drastically higher than Belka, it is making to 19.4%, 14.2% and 0.7% respectively. In the tracheobronchial region, the maximum deposition fraction achieved by $S - N$ and $T - C$ drag model is found in the region LLL1(denoted by 3) yielded values 11.4%, 12.2%, on the other

hand the highest deposition fraction of 15.0 % is seen in region RLL1 (denoted by 9) of Belka results. The least deposition fraction is in LUL1 (denoted by 1) for all. [59]
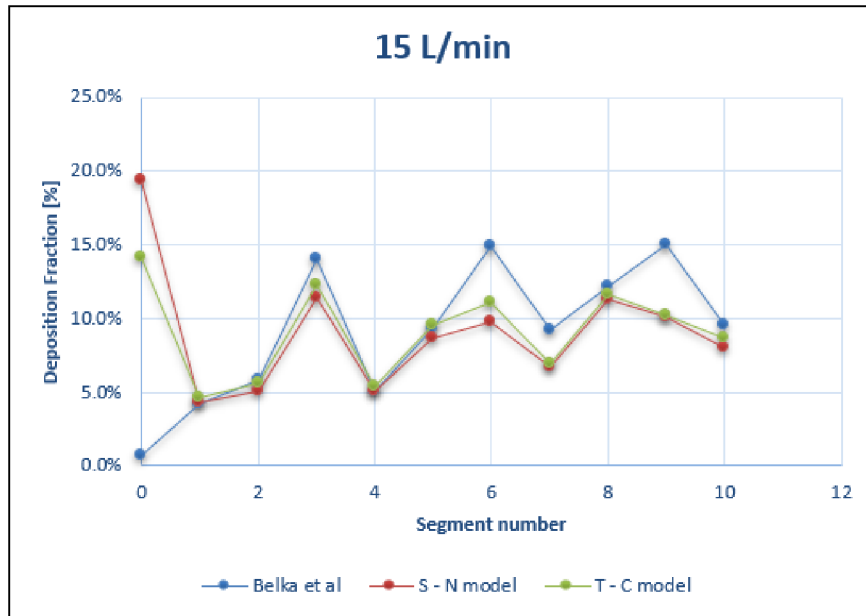

Figure 24: deposition fraction of flow rate 15 L/min, Belka vs. S - N drag model vs. T - C drag model.

It is demonstrated in the results, regional deposition values obtained by T − C drag model is moderately higher than S − N drag model and the curve shows Belka's approach yields even higher values, this could be because of higher values of drag force in the T − C drag model and Belka's Approach. Although, there is less deposition fraction is seen in oropharyngeal-laryngeal region in Belka's model but in tracheobronchial region deposition fraction is higher than S − N and T − C, more specifically in segment 2, 3, 6, 7, 8, 9, 10. [59]

In oral airway, inertial impaction is the dominating deposition mechanism due to the turbulent flow and particles can deposit in the oral cavity and pharynx. In trachea, the deposition is again due to the turbulence flow regime causing fiber to accelerate and impact with the walls. In bronchial region, in fig. 22, region 3, 6, 7, 8 velocities are higher in that region hence that influence deposition by impaction.[61]

6. Conclusion

There is significant research performed experimentally and numerically in particle deposition and its transport though different models, but our choice of model is unique and complex due to intricacy of respiratory tract and its measurement challenges. The extensive literature review in this project states that there are many experimental investigations done by many researchers which are focused on the deposition and transport of fiber particles experimentally and to validate these experimental studies numerical simulations are a correct approach to this research. The main purpose of this project is to gather information from experiments and utilize it in numerical simulation. To achieve that we performed CFD-DEM simulation and evaluated $T-C$ approach to validated experimental study of Lizal and Belka.

The goal is achieved by evaluating two different kinds of geometry, one has single bifurcation called Y-model and the other geometry has many bifurcations up to generation 7 model of human respiratory tract. We considered different dimensions of the particles and concluded that longitudinal particles such as particle clumps experience different drag coefficient w.r.t spherical particles.

The main approach which is useful for this investigation is the lagrangian approach, which makes it possible to track the particles. For the Y model, CFD – DEM approach is selected to visualize and analyze the behaviour of fiber particles and concluded that to accurately monitor the particles, we must include three DEM criteria which are particle velocity, collision duration and Rayleigh time. Despite the fact we take these criteria into account, it takes an enormously long time to calculate the particles motion which is not very suitable for application.

For the realistic model of human airway, a modified drag coefficient lagrangian framework was used, in which drag coefficient was modified using $T-C$ approach because it considers dimensional parameters of the particles more accurately, however it is not able to describe the real behaviour of the fiber particles. In our simulation, the fiber is perpendicular to the streamlines which simplifies the calculations however, it is not reasonable approximation for certain scenarios. It is important to note that this assumption may not hold true for the entire

trajectory in complex flow field. Particles are subject to experience rotation which can lead them to follow different trajectories.

The approach used in this investigation proves to be a great methodology to monitor deposition fraction and have the potential for further development in the future. Firstly, the model geometry can be more realistic to avoid inaccuracy in boundary conditions or there could be more options in the software while prescribing a detailed boundary condition. Secondly, in terms of particles, it is known that fiber particles are more dangerous than spherical particles, it is possible to add new range of fiber particle size and shapes to increase the variety of particles. I recommend these possibilities for further development but there are certainly several other possibilities which can also be taken into account.

7. References

1. ASGHARIAN, Bahman, T.Price OWEN, Eileen.D KUEMPEL, and Annie M. JARABEK. Toxicology and Applied Pharmacology. Dosimetry of inhaled elongated mineral particles in the respiratory tract. The impact of shape factor. 1 May 2018 l., 12 January 2018 (0041-008X), 27 - 35.

2. P.A. Cundall, O. Strack, A discrete numerical model for granular assemblies, Geotechnique 29 (1) (1979) 47–65.

3. CHEN, Xiaole, Wenqi ZHONG, Xianguang ZHOU, Baosheng JIN a Baobin SUN. CFD–DEM simulation of particle transport and deposition in pulmonary airway. Powder Technology [online]. 2012, 228, 309-318 [cit. 2023-04-27]. ISSN 00325910. Dostupné z: doi:10.1016/j.powtec.2012.05.041

4. LIZAL, Frantisek, Matous CABALKA, Milan MALY, et al. On the behavior of inhaled fibers in a replica of the first airway bifurcation under steady flow conditions. Aerosol Science and Technology [online]. 2022, 56(4), 367-381 [cit. 2023-04-27]. ISSN 0278-6826. Dostupné z: doi:10.1080/02786826.2022.2027334

5. Tian, L. and G. Ahmadi. 2013. Fiber transport and deposition in human upper tracheobronchial airways. J. Aerosol Sci. 60:1–20. doi:10.1016/j.jaerosci.2013.02.001.

6. Zastawny, M., G. Mallouppas, F. Zhao, and B. van Wachem. 2012. Derivation of drag and lift force and torque coefficients for non-spherical particles in flows. Int. J.Multiphase Flow 39:227–239. doi:10.1016/j.ijmultiphase-flow.2011.09.004.

7. Aerosols : Tiny Particulates in the Air. UCAR | Center for Science and Education [online]. 2021 [cit. 2023-04-27]. Available from: https://scied.ucar.edu/learning-zone/air-quality/aerosols.

8. Yaowei Li, Longyi Shao, Wenhua Wang, Mengyuan Zhang, Xiaolei Feng, Wenjun Li, Daizhou Zhang, Airborne fiber particles: Types, size and concentration observed in Beijing, Science of The Total Environment, Volume 705, 2020, 135967, https://doi.org/10.1016/j.scitotenv.2019.135967.

9. DARQUENNE, Chantal. Deposition Mechanisms. Journal of Aerosol Medicine and Pulmonary Drug Delivery [online]. 2020, 33(4), 181-185 [cit. 2023-04-27]. ISSN 1941-2711. Dostupné z: doi:10.1089/jamp.2020.29029.cd

10. KLEINSTREUER, Clement a Yu FENG. Computational Analysis of Non-Spherical Particle Transport and Deposition in Shear Flow With Application to Lung Aerosol Dynamics—A Review. Journal of Biomechanical Engineering [online]. 2013, 135(2) [cit. 2023-04-27]. ISSN 0148-0731. Dostupné z: doi:10.1115/1.4023236

11. TU, Jiyuan, Kiao INTHAVONG a Goodarz AHMADI. Computational Fluid and Particle Dynamics in the Human Respiratory System [online]. Dordrecht: Springer Netherlands, 2013 [cit. 2023-04-27]. Biological and Medical Physics, Biomedical Engineering. ISBN 978-94-007-4487-5. Dostupné z: doi:10.1007/978-94-007-4488-2

12. HARRIS, ROBERT L. a DAVID A. FRASER. A model for deposition of fibers in the human respiratory system. American Industrial Hygiene Association Journal [online]. 2010, 37(2), 73-89 [cit. 2023-04-27]. ISSN 0002-8894. Dostupné z: doi:10.1080/0002889768507416.

13. MYOJO, Toshihiko. Deposition of fibrous aerosol in model bifurcating tubes. Journal of Aerosol Science [online]. 1987, 18(3), 337-347 [cit. 2023-04-27]. ISSN 00218502. Dostupné z: doi:10.1016/0021-8502(87)90027-9

14. ZHOU, Yue a Yung-Sung CHENG. Particle Deposition in a Cast of Human Tracheobronchial Airways. Aerosol Science and Technology [online]. 2005, 39(6), 492-500 [cit. 2023-04-27]. ISSN 0278-6826. Dostupné z: doi:10.1080/027868291001385

15. MYOJO, Toshihiko a Mitsutoshi TAKAYA. Estimation of Fibrous Aerosol Deposition in Upper Bronchi Based on Experimental Data with Model Bifurcation. INDUSTRIAL HEALTH [online]. 2001, 39(2), 141-149 [cit. 2023-04-27]. ISSN 0019-8366. Dostupné z: doi:10.2486/indhealth.39.141

16. SUSSMAN, Robert G., Beverly S. COHEN a Morton LIPPMANN. Asbestos Fiber Deposition in a Human Tracheobronchial Cast. I. Experimental. Inhalation Toxicology [online]. 2008, 3(2), 145-160 [cit. 2023-04-28]. ISSN 0895-8378. Dostupné z: doi:10.3109/08958379109145281

17. SU, Wei-Chung, Bon Ki KU, Pramod KULKARNI a Yung Sung CHENG. Deposition of graphene nanomaterial aerosols in human upper airways. Journal of Occupational and Environmental Hygiene [online]. 2016, 13(1), 48-59 [cit. 2023-04-28]. ISSN 1545-9624. Dostupné z: doi:10.1080/15459624.2015.1076162

18. NIELSEN, G.D. a I.K KOPONEN. Insulation fiber deposition in the airways of men and rats. A review of experimental and computational studies. Regulatory Toxicology and Pharmacology [online]. 2018, 94, 252-270 [cit. 2023-04-28]. ISSN 02732300. Dostupné z: doi:10.1016/j.yrtph.2018.01.021

19. ZHOU, Yue, Wei-Chung SU a Yung Sung CHENG. Fiber Deposition in the Tracheobronchial Region: Deposition Equations. Inhalation Toxicology [online]. 2008, 20(13), 1191-1198 [cit. 2023-04-28]. ISSN 0895-8378. Dostupné z: doi:10.1080/08958370802233082

20. LIZAL Frantisek, Jakub ELCNER, Philip K HOPKE, Jan JEDELSKY a Miroslav JICHA. Development of a realistic human airway model. Proceedings of the Institution of Mechanical Engineers, Part H: Journal of Engineering in Medicine [online]. 2012, 226(3), 197-207 [cit. 2023-04-28]. ISSN 0954-4119. Dostupné z: doi:10.1177/0954411911430188

21. FRANTISEK, Lizal, Jakub ELCNER, Miloslav BELKA, Jan JEDELSKY, Philip K. HOPKE, Pavel STARHA, Hana DRUCKMULLEROVA and Miroslav JICHA. Measurement of Fiber Deposition in a Human Lung Model by Phase Contrast Microscopy with Automated Image Analysis. Engineering Mechanics. April 18, 2013, October 15, 2012 , 187.

22. Two-Phase Flow [online]. Routledge, 2017 [cit. 2023-04-28]. ISBN 9780203734865. Dostupné z: doi:10.1201/9780203734865

23. HU, H.H. Direct simulation of flows of solid-liquid mixtures. International Journal of Multiphase Flow [online]. 1996, 22(2), 335-352 [cit. 2023-04-28]. ISSN 03019322. Dostupné z: doi:10.1016/0301-9322(95)00068-2

24. CHEN, Xiaole, Wenqi ZHONG, Xianguang ZHOU, Baosheng JIN a Baobin SUN. CFD–DEM simulation of particle transport and deposition in pulmonary airway. Powder Technology [online]. 2012, 228, 309-318 [cit. 2023-04-28]. ISSN 00325910. Dostupné z: doi:10.1016/j.powtec.2012.05.041

25. TAO, He, Baosheng JIN a Wenqi ZHONG. Simulation of ellipsoidal particle flow in rectangular hopper with discrete element method. In: 2011 International Conference on Electric Technology and Civil Engineering (ICETCE) [online]. IEEE, 2011, 2011, s. 678-

681 [cit. 2023-04-28]. ISBN 978-1-4577-0289-1. Dostupné z: doi:10.1109/ICETCE.2011.5776032

26. CHENG, Kaiwen, Jingjing ZHU, Fuping QIAN, Bowen CAO, Jinli LU a Yunlong HAN. CFD–DEM simulation of particle deposition characteristics of pleated air filter media based on porous media model. Particuology [online]. 2023, 72, 37-48 [cit. 2023-04-28]. ISSN 16742001. Dostupné z: doi:10.1016/j.partic.2022.02.003

27. HUANG, Fen, Qixuan ZHU, Xudong ZHOU, Dazhao GOU, Jiaqi YU, Renjie LI, Zhenbo TONG a Runyu YANG. Role of CFD based in silico modelling in establishing an in vitro-in vivo correlation of aerosol deposition in the respiratory tract. Advanced Drug Delivery Reviews [online]. 2021, 170, 369-385 [cit. 2023-04-28]. ISSN 0169409X. Dostupné z: doi:10.1016/j.addr.2020.09.007

28. KIASADEGH, Morteza, Homayoun EMDAD, Goodarz AHMADI a Omid ABOUALI. Transient numerical simulation of airflow and fibrous particles in a human upper airway model. Journal of Aerosol Science [online]. 2020, 140 [cit. 2023-04-28]. ISSN 00218502. Dostupné z: doi:10.1016/j.jaerosci.2019.105480

29. VAN WACHEM, Berend, Marian ZASTAWNY, Fan ZHAO a George MALLOUPPAS. Modelling of gas–solid turbulent channel flow with non-spherical particles with large Stokes numbers. International Journal of Multiphase Flow [online]. 2015, 68, 80-92 [cit. 2023-04-28]. ISSN 03019322. Dostupné z: doi:10.1016/j.ijmultiphaseflow.2014.10.006

30. ZHONG, Wenqi, Aibing YU, Xuejiao LIU, Zhenbo TONG a Hao ZHANG. DEM/CFD-DEM Modelling of Non-spherical Particulate Systems: Theoretical Developments and Applications. Powder Technology [online]. 2016, 302, 108-152 [cit. 2023-04-29]. ISSN 00325910. Dostupné z: doi:10.1016/j.powtec.2016.07.010

31. AHOOKHOSH, Kaveh, Oveis POURMEHRAN, Habib AMINFAR, Mousa MOHAMMADPOURFARD, Mohammad Mohsen SARAFRAZ a Hamed HAMISHEHKAR. Development of human respiratory airway models: A review. European Journal of Pharmaceutical Sciences [online]. 2020, 145 [cit. 2023-04-30]. ISSN 09280987. Dostupné z: doi:10.1016/j.ejps.2020.105233

32. SOSNOWSKI, Marcin, Renata GNATOWSKA, Jacek SOBCZYK a Waldemar WODZIAK. Computational domain discretization for CFD analysis of flow in a granular

packed bed. Journal of Theoretical and Applied Mechanics [online]. 2019, 57(4), 833-842 [cit. 2023-05-01]. ISSN 1429-2955. Dostupné z: doi:10.15632/jtam-pl/112017

33. In: Polyhedral Mersher: HELP : Simcenter STAR CCM+ [online]. [feeling. 2023-05-01]. Available from:

file:///H:/CCM+%20New%20Version/Installation%20Setup%20file%20(Usman)/17.06.0 07-R8/STAR-CCM+17.06.007-R8/doc/en/online/

index.html#page/STARCCMP%2FGUID-812361C5-EEF9-4028-8A9C-EF5F730917B6.html%23

34. What is a Parcel?. In: Simcenter [online]. [feeling. 2023-05-03]. Available from:

file:///H:/CCM+%20New%20Version/Installation%20Setup%20file%20(Usman)/17.06.0 07-R8/STAR-CCM+17.06.007-R8/doc/en/online/

index.html#page/STARCCMP%2FGUID-4876089D-B45F-4967-94B0-61A16011F41B.html%23wwID0ENAX2B

35. Using the Lagrangian Multiphase Model with Time Models. In: Simcenter STAR CCM + [online]. [feeling. 2023-05-03]. Available from:

file:///H:/CCM+%20New%20Version/Installation%20Setup%20file%20(Usman)/17.06.0 07-R8/STAR-CCM+17.06.007-R8/doc/en/online/

index.html#page/STARCCMP%2FGUID-A0F95175-BC05-45A5-958E-B7F6B38A0BFC.html%23

36. TRAN-CONG, Sabine, Michael GAY a Efstathios E MICHAELIDES. Drag coefficients of irregularly shaped particles. Powder Technology [online]. 2004, 139(1), 21-32 [cit. 2023-05-03]. ISSN 00325910. Dostupné z: doi:10.1016/j.powtec.2003.10.002

37. In: Eulerian Multiphase (EMP): HELP : Simcenter STAR CCM+ [online]. [feeling. 2023-05-01]. Available from:

file:///H:/CCM+%20New%20Version/Installation%20Setup%20file%20(Usman)/17.06.0 07-R8/STAR-CCM+17.06.007-R8/doc/en/online/

index.html#page/STARCCMP%2FGUID-9F7F7EF1-F1B0-458A-9082-4233E522AA36.html%23

38. In: Discrete Element Method (DEM): HELP : Simcenter STAR CCM+ [online]. [feeling. 2023-05-01]. Available from:

file:///H:/CCM+%20New%20Version/Installation%20Setup%20file%20(Usman)/17.06.0
07-R8/STAR-CCM+17.06.007-R8/doc/en/online/
index.html#page/STARCCMP%2FGUID-68BB8A6E-63A6-4BC2-89D0-
A1B84B95A18D.html%23

39. In: Speeding up DEM Particle Clumps Simulation: Simcenter Support Center [online].
[feeling. 2023-05-01]. Available from: https://support.sw.siemens.com/cs-
CZ/knowledge-base/KB000038940_EN_US

40. FARKAS, Árpád, Frantisek LIZAL, Jakub ELCNER, Jan JEDELSKY a Miroslav
JICHA. Numerical simulation of fibre deposition in oral and large bronchial airways in
comparison with experiments. Journal of Aerosol Science [online]. 2019, 136, 1-14 [cit.
2023-05-04]. ISSN 00218502. Dostupné z: doi:10.1016/j.jaerosci.2019.06.003

41. Schmidt, A., Zidowitz, S., Kriete, A., Denhard, T., Krass, S., & Peitgen, H. O. (2004). A
digital reference model of the bronchial tree. Computerized Medical Imaging and
Graphics, 28, 203–211.

42. Lizal, F., Elcner, J., Hopke, P. K., Jedelsky, J., & Jicha, M. (2012). Development of a
realistic human airway model. Proceedings of the Institution of Mechanical Engineers -
Part H: Journal of Engineering in Medicine, 226, 197–207.

43. Discrete Element Method (DEM). Simcenter STAR - CCM+ [online]. [feeling. 2023-05-
07]. Available from: file:///D:/Simcenter%20STAR
CCM+%20Discrete%20Element%20Method%20(DEM)%20-
%20Technology%20Spotlight%20Presentation.pdf

44. Contact Force. Simcenter STAR - CCM+ [online]. [feeling. 2023-05-07]. Available
from:
file:///H:/CCM+%20New%20Version/Installation%20Setup%20file%20(Usman)/17.06.0
07-R8/STAR-CCM+17.06.007-R8/doc/en/online/
index.html#page/STARCCMP%2FGUID-D9FD8743-D2A9-4705-87AF-
BB88B9BDDA58.html%23wwID0EKMXUD

45. Bonded Particles Model Reference. Simcenter STAR - CCM+ [online]. [feeling. 2023-
05-07]. Available from:
file:///H:/CCM+%20New%20Version/Installation%20Setup%20file%20(Usman)/17.06.0

07-R8/STAR-CCM+17.06.007-R8/doc/en/online/

index.html#page/STARCCMP%2FGUID-DD570218-D7F7-4F93-A903-

0A39F2ED4324.html%23

46. Hertz Mindlin Model Reference. Simcenter STAR - CCM+ [online]. [feeling. 2023-05-
07]. Available from:

file:///H:/CCM+%20New%20Version/Installation%20Setup%20file%20(Usman)/17.06.0

07-R8/STAR-CCM+17.06.007-R8/doc/en/online/

index.html#page/STARCCMP%2FGUID-F0AF9D14-EBC7-4EEE-B795-

510BEA25BF4B.html%23

47. Rolling Resistance Model Reference. Simcenter STAR - CCM+ [online]. [feeling. 2023-
05-07]. Available from:

file:///H:/CCM+%20New%20Version/Installation%20Setup%20file%20(Usman)/17.06.0

07-R8/STAR-CCM+17.06.007-R8/doc/en/online/

index.html#page/STARCCMP%2FGUID-33C135CF-079E-4687-B7C7-

59DAE0D78E9E.html%23

48. World Health Organization (WHO), Determination of airborne fibre number
concentrations, A recommended method by phase-contrast optical microscopy
(membrane filter method), Geneva: WHO, 2000.

49. IARC, 1977. IARC Monographs on the Evaluation of Carcinogenic Risk of Chemicals to
Man: Asbestos. vol. 14 World Health Organization, International Agency for Research on
Cancer, Lyon, France Available at: http://monographs.iarc.fr/ENG/Monographs/vol1-
42/mono14.pdf.

50. IARC, 1989. In: Bignon, J., Peto, J., Saracci, R. (Eds.), Non-occupational Exposure to
Mineral Fibres. IARC Scientific Publications No. 90. World Health Organization,
International Agency for Research on Cancer, Lyon, France Available at:
http://www.iarc.fr/en/publications/pdfs-online/sp90/.

51. IARC, 2002. IARC Monographs on the Evaluation of Carcinogenic Risks to Humans:
Man-made Vitreous Fibres. vol. 81 World Health Organization, International Agency for
Research on Cancer, Lyon, France Available at:
http://monographs.iarc.fr/ENG/Monographs/vol81/mono81.pdf.

52. IARC, 2012. IARC Monographs on the Evaluation of Carcinogenic Risks to Humans: Arsenic, Metals, Fibres, and Dusts. A Review of Human Carcinogens, vol. 100C World Health Organization, International Agency for Research on Cancer, Lyon, France Available at: http://monographs.iarc.fr/ENG/Monographs/vol100C/mono100C.pdf.

53. Yasunosuke Suzuki, Norihiko Kohyama, Malignant mesothelioma induced by asbestos and zeolite in the mouse peritoneal cavity, Environmental Research, Volume 35, Issue 1, 1984, Pages 277 - 292, ISSN 0013-9351, https://doi.org/10.1016/0013-9351(84)90136-1

54. ICRP, 1994. Human Respiratory Tract Model for Radiological Protection. Publication 66. International Commission on Radiological Protection. 24. Pergamon Press, Oxford, United Kingdom, pp. 272 Annals of ICRP.

55. Center for Science Education (no date) Aerosols: Tiny Particulates in the Air | Center for Science Education. Available at: https://scied.ucar.edu/learning-zone/air-quality/aerosols (Accessed: February 7, 2023).

56. CCOHS. (n.d.). How do particulates enter the respiratory system? Canadian Center of Occupational Health and Safety; CCOHS. Retrieved June 5, 2022, from https://www.ccohs.ca/oshanswers/chemicals/how_do.html

57. FARKAS, Árpád, Frantisek LIZAL, Jakub ELCNER, Jan JEDELSKY a Miroslav JICHA. Numerical simulation of fibre deposition in oral and large bronchial airways in comparison with experiments. Journal of Aerosol Science [online]. 2019, 136, 1-14 [cit. 2023-05-13]. ISSN 00218502. Dostupné z: doi:10.1016/j.jaerosci.2019.06.003

58. Local DEM Time Stepping. Siemens Support Center [online]. [feeling. 2023-05-14]. Available from: https://support.sw.siemens.com/cs-CZ/knowledge-base/KB000038940_EN_US

59. BELKA, Miloslav, Frantisek LIZAL, Jan JEDELSKY, Jakub ELCNER, Philip K. HOPKE a Miroslav JICHA. Deposition of glass fibers in a physically realistic replica of the human respiratory tract. Journal of Aerosol Science [online]. 2018, 117, 149-163 [cit. 2023-05-17]. ISSN 00218502. Dostupné z: doi:10.1016/j.jaerosci.2017.11.006

60. LIZAL, Frantisek, Jakub ELCNER, Philip K HOPKE, Jan JEDELSKY a Miroslav JICHA. Development of a realistic human airway model. Proceedings of the Institution of Mechanical Engineers, Part H: Journal of Engineering in Medicine [online]. 2012,

226(3), 197-207 [cit. 2023-05-17]. ISSN 0954-4119. Dostupné z:

doi:10.1177/0954411911430188

61. Aerosol transport and deposition in the human respiratory tract [online]. 2015 [cit. 2023-

05-18]. Available from:

file:///C:/Users/USMAN/OneDrive/Desktop/Elcner_dizertace_compressed%20(1).pdf

8. Nomenclature

Symbols	Description
CFD	Computational Fluid Dynamics
DEM	Discrete element method
LA	Lagrangian Approach
SEM	Scanning Electron Microscope
EDX	Energy Dispersive X-Ray
MMMF	Man Made Mineral Fiber
C	Carbon
O	Oxygen
Ca	Calcium
S	Sulfur
Mg	Magnesium
Al	Aluminum
Si	Silicon
P	Phosphorus
Fe	Iron
Ti	Titanium
Na	Sodium
CNS	Complete Numerical Simulation
DNS	Direct Numerical Simulation
ALE	Arbitrary Lagrangian Eulerian
DLM	Distributed Lagrangian Multiplier
EL – ER	Euler Lagrange – Euler Rotation
CNT	Carbon Nano Tube
TiO_2	Titanium Dioxide
IVIVC	In Vitro – In Vivo Correlation
NSPS	Non-Spherical Particulate System
CT	Computed Tomography

MRI	Magnetic Resonance Imaging
LMP	Lagrangian Multiphase
T − C	Tran Cong
H − L	Haider and Levenspiel

9. List of Figures

10.   List of Tables